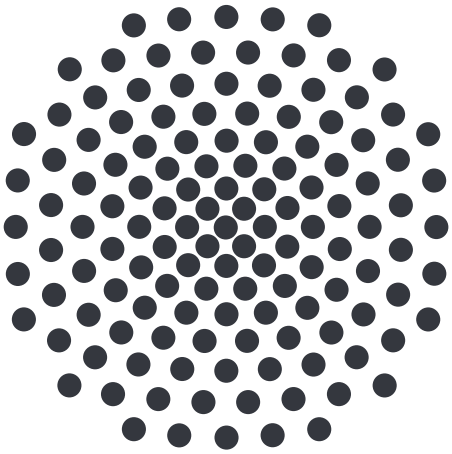

University of Stuttgart

Institute for Theoretical Physics III

Master Thesis

Quantum Hall Tunneling of Cold Atomic Gases

Daniel Bidlingmaier

1st Supervisor: Prof. Dr. Hans Peter Büchler
2nd Supervisor: Prof. Dr. Maria Daghofer

January 11, 2023

Declaration

I declare that I have developed and written the enclosed Master Thesis completely by myself, and have not used sources or means without declaration in the text. Any thoughts from others or literal quotations are clearly marked. The Master Thesis was not used in the same or in a similar version to achieve an academic grading or is being published elsewhere. Lastly, I assure that the electronic copy of this Master Thesis is identical in content with the enclosed version.

Stuttgart, January 11 , 2023

Abstract

English

An electron on a plane in the presence of a perpendicular magnetic field follows circular orbits. A quantum mechanical treatment shows that the energy corresponding to these orbits is quantized into discrete and highly degenerate Landau levels. For low energies and strong magnetic fields the electron is forced into the lowest Landau level. Recent experiments have been able to realize this in an equivalent system using a Bose-Einstein condensate confined by a rotating trap [1]. We study the dynamics in the lowest Landau level in the presence of an external potential specifically we consider tunneling in a periodic potential.

We start by introducing new coordinates and projecting onto the lowest Landau level which allows us to treat the system as quasi one-dimensional in the path integral. We use complex instanton solutions to the Euler Lagrange equations in order to calculate the instanton action of the related tunneling process. We show that the imaginary part of the instanton action for closed paths agrees with the predicted Aharanov-Bohm phase. We find that the instanton action and therefore the tunneling probability is independent from the height of the potential. The spreading of a wavefunction should then be dictated by geometric effects. This motivates the second part of this thesis in which we discuss the time evolution of a particle on a square lattice in a magnetic field. We investigate how changes in the magnetic field can influence the speed with which the particle spreads. We compare analytical results with results obtained using continuous quantum random walks. We find that the rationality of the Aharanov Bohm phase for one loop around a unit cell plays a key role in the long term behaviour of the particle.

Deutsch

Ein Elektron in einer Ebene wird mit einem orthogonalen magnetischen Feld bewegt sich auf einer Kreisbahn. Eine quantenmechanische Betrachtung des Systems zeigt, dass die Energieniveaus welche mit den Orbits zusammenhängen in diskrete und stark entartete Landau Level quantisiert sind. Für starke Magnetfelder und geringe Energien wird das Elektron in das niedrigste Landau Level gezwungen. In aktuellen Experimenten wird stattdessen auch die Äquivalenz zwischen rotierenden Systemen verwendet, wie zum Beispiel bei dem ein Bose-Einstein Kondensat in einer rotierenden Falle [1]. Ziel dieser Arbeit ist es die Dynamik eines Teilchen im niedrigsten Landau Level in der Gegenwart eines zusätzlichen Potentials zu untersuchen, speziell Tunneln in einem periodischen Potential .

Zuerst transformieren wir auf neue Koordinaten und projizieren anschließend auf das unterste Landau Level, auf diese Art kann das System als quasi eindimensional im Pfadintegralformalismus aufgefasst werden. Wir bestimmen komplexe Instanton-Lösungen der Euler Lagrange Gleichungen und verwenden diese um die Instantonenwirkung zu bestimmten Tunnelereignissen zu berechnen. Wir zeigen, dass der imaginäre Teil der Instantonenwirkung für geschlossene Pfade mit der erwarteten Aharanov-Bohm Phase übereinstimmt. Die Instantonenwirkung und somit die Tunnelrate, ist nicht von der Potentialhöhe abhängig. Die Ausbreitung einer Wellenfunktion wird deshalb von geometrischen Effekten diktiert. Aus diesem Grund beschäftigt sich der zweite Teil dieser Arbeit mit der zeitlichen Ausbreitungen eines Teilchens auf einem quadratischen Gitter.

Dabei untersuchen wir den Einfluss des magnetischen Felds auf die Ausbreitungsgeschwindigkeit. Die numerisch durch kontinuierliche Quantum Walks erhaltene Ergebnisse vergleichen wir mit analytischen Berechnungen. Es zeigt sich, dass die Rationalität der beim Umlauf um eine Gitterzelle erhaltene Aharanov-Bohm Phase die Ausbreitungsgeschwindigkeit bei Betrachtung langer Zeiten signifikant beeinflusst.

Contents

1. Introduction

In this chapter we highlight the general structure of this thesis and give a short introductionary overview for each of the following chapters. Each chapter will also start with a quick introduction and end with a brief summary.

We begin chapter 2 by introducing the system of interest, namely an electron moving in a plane in the presence of an orthogonal magnetic field. In section 2.1 we discuss the gauge invariance of the system as well as the shape of the Hamiltonian in the symmetric and in the Landau gauge. Additionally a short explanation of Landau quantization is given and the form of wave functions in the lowest Landau level is discussed. Section 2.2 deals with the Aharanov-Bohm phase of an electron moving along a closed path around a confined magnetic field .

In section 2.3 we discuss an equivalent system, a Bose-Einstein condensate confined by a rotating trap experimentally realized in [1]. We highlight the correspondence between the systems and their respective length scales. At this point we also introduce cyclotron and guiding center coordinates and discuss their new commutation relations. In section 2.4 we discuss how an additional potential can be projected onto the lowest energy level of the cyclotron coordinates. This way the potential is now only a function of the two guiding center coordinates. Due to their commutator they can be interpreted as a spatial coordinate and its corresponding momentum. We briefly address the issue of operator ordering, and argue that it would be sensible to use Weyl ordering in order to be consistent with the path integral formalism. Projecting onto the lowest energy level involves the convolution of the original potential with a Gaussian function, and we explain how this affects certain classes of functions.

Chapter 3 introduces the instanton technique which we will later use to tackle tunneling problems. Here we look at the double well potential as its a simpler yet instructive example how the instanton formalism can be applied to tunneling problems. We explicitly calculate the instanton and anti-instanton trajectories, together with the instanton action and the tunneling probability. This is followed by a discussion of the dilute gas approximation and its application for calculating the partition function.

In chapter 4 we study an electron in a periodic potential, for which we study the model Hamiltonian $\hat{H}(x,y) = 2 - \cos(x) - \cos(y)$, where y (or alternatively x) can be interpreted as the momentum operator. Section 4.1 starts with the formulation of the Euler-Lagrange equations, where we see that if we allow one coordinate to be complex we get equipotential lines connecting the minima of the Hamiltonian. We find instanton solutions for all types of nearest neighbour tunneling processes (namely x- and y- instanton and anti-instantons starting at an arbitrary minimum). We also analyze how those solutions change when the coordinates are rescaled and a prefactor is introduced.

In section 4.2 we continue by calculating the action for the different types of instantons. And discuss how the imaginary part of the instanton action depends on the type of instanton. We come back to these results in section 4.4 where we investigate which phases are related to the tunneling events and show that the path dependent phases stem from the imaginary part of the instanton action. We confirm that this phase agrees with the predicted Aharanov-Bohm phase.

In section4.3 we follow the calculations done in [5] where the partition function together with the energy corrections due to tunneling are computed. At the end of this section

we briefly discuss Bloch angles and the so-called Hofstadter Butterfly which refers to the energy spectrum of this system.

Chapter 5 opens the second part of this thesis where we start with a localized state and investigate how its spreading during the time evolution. Section 5.1 starts with the Hamiltonian of a linear chain where only nearest neighbour tunneling is allowed. After diagonalizing it using the Fourier transform we proceed to extend this result to the two dimensional counterpart, a square lattice. We also show how introducing the phases discussed in section 4.4 changes the Hamiltonian. In this case we are not able to fully diagonalize the Hamiltonian. In absence of the phase induced by the magnetic field we calculate the time evolution for a state which is localized at $t = 0$ at one of the lattice sites. We show that the probability amplitudes care given by Bessel functions. We conclude this section by looking at the case of an unconstricted free particle. The starting state is chosen to be Gaussian wave packet centered around the origin. The time evolution shows that the wave packet keeps its shape but its width increases over time.

Section 5.2 starts with an short introduction into quantum random walks. In the remainder of this section we use the continuous quantum random walk to investigate the same questions as in section 5.1. First we consider the case where additional phases are absent. We use the zeros of the Bessel functions to compare the analytical result with the probability distribution we obtained numerically. We find that the average distance grows linear in time, which is a key feature distinguishing quantum random walks from classical random walks.

Our numerical calculations only consider a square lattice of finite size which makes assessing potential finite size effects necessary. Following this tunneling phases are introduced and the same calculations are repeated. We find that the interference between tunneling paths with same starting and end point now significantly influences the speed of the spreading. Our numerical analysis shows that the state spreads faster at large times if the magnetic flux per unit cell is close to rational multiple of 2π with small denominator. We end section 5.2 by comparing the different cases and regimes we looked at in this chapter. This is followed by a summarizing conclusion in chapter 6.

2. Single Electron in a Magnetic Field

This chapter gives an introduction into the theory of behind Landau quantization. A thorough discussion of this can be found in [4]. We highlight the role of the gauge and how an electron moving in a magnetic field picks up a phase which depends on the magnetic flux. In the next section we explain how systems with neutral atoms in rotating traps are connected to systems with charged particles in magnetic fields. This is followed by transforming onto cyclotron and guiding center coordinates. The last section of this chapter explains how we get an effective potential by projecting onto the lowest Landau level.

2.1. Landau Quantization

We start by considering a single electron restricted in such a way that it can only move on a plane. This will be the basic setup underlying all of the calculations done in later chapters. A particle with charge q within a magnetic field can be described by the following Hamiltonian

$$\hat{H} = \frac{1}{2m}|\hat{p} - q\hat{A}|^2, \tag{1}$$

where $\hat{A}$ is the magnetic vector potential, which is related to the magnetic field by $\mathbf{B} = \nabla \times \hat{A}$. One should keep in mind that due to gauge freedom multiple vector potentials $\hat{A}$ can correspond to the same magnetic field. In our case we are interested in a constant magnetic field perpendicular to the plane in which the electron is confined. For the magnetic Field $\mathbf{B} = B\mathbf{e}_z$ two examples of different corresponding magnetic vector potentials would be

$$\text{Landau gauge: } \hat{A} = \begin{pmatrix} 0 \\ Bx \\ 0 \end{pmatrix} \qquad \text{symmetric gauge: } \hat{A} = \frac{1}{2}\begin{pmatrix} -By \\ Bx \\ 0 \end{pmatrix} \tag{2}$$

Choosing the Landau gauge the Hamiltonian from (1) now reads

$$\hat{H} = \frac{p_x^2}{2m} + \frac{1}{2m}(p_y - qBx)^2 + \frac{p_z^2}{2m}. \tag{3}$$

The last term in this Hamiltonian corresponds to the movement of the particle in z-direction and since we assume that a trap restricts the movement onto the xy-plane this term can be omitted. We additionally impose restrictions on the other coordinates namely $0 \leq x \leq L_x$ und $0 \leq y \leq L_y$. Through the introduction of the cyclotron frequency $\omega_c = qB/m$ and the eigenvalues $\hbar k_y$ of $\hat{p_y}$ we can rewrite the Hamiltonian as

$$\hat{H} = \frac{p_x^2}{2m} + \frac{1}{2}m\omega_c^2(x - \frac{\hbar k_y}{m\omega_c})^2. \tag{4}$$

The Hamiltonian in (4) possesses the same form as the Hamiltonian of a 1D harmonic oscillator where the spacial coordinate got a shift. Therefore we get also get the energy levels $E_n = \hbar\omega_c(n + 1/2)$ of the harmonic oscillator. Notably the energy levels do not depend on the quantum number k_y. Hence the energy levels (Landau levels) are degenerate with k_y being able to take the values $2\pi N/L_y$ where N is an integer between 0 and $m\omega_c L_x L_y/(2\pi\hbar)$. Due to $w_c \propto B$ an increase of the magnetic field also increases the number of values k_y can take for a given Landau level as well as the energy gap between Landau levels. Ensuring that the energy in the system is low combined with

a sufficiently strong magnetic field one can ensure that the entire dynamic of the system takes places in the lowest Landau level ($n = 0$). We will make use of this fact later on.

The magnetic field also introduces Zeeman-splitting in the case of an electron. Again for a strong enough magnetic field and sufficiently low energy the Zeeman splitting is large and the electron is forced into the spin configuration with lower energy. For this reason we will not concern ourselves further with Zeeman splitting.

Instead of choosing the Landau gauge we can also choose the symmetric gauge in which case we get the Hamiltonian

$$\hat{H} = \frac{1}{2m}\left(p_x + \frac{qBy}{2}\right)^2 + \frac{1}{2m}\left(p_y - \frac{qBx}{2}\right)^2 \tag{5}$$

The wave functions for the lowest Landau level in symmetric gauge have the form

$$\Psi(x,y) = f(x - iy)e^{-(x^2+y^2)/(4l_\mathrm{B}^2)} \tag{6}$$

where f is an analytic function, $l_\mathrm{B} = \sqrt{\hbar/eB}$ is the magnetic length and e relates to the electron charge by $q_\mathrm{electron} = -e$. The magnetic length will play an important role later on as it is the length scale of this system. The Gaussian shaped ground state wave function will be needed when projecting onto the lowest Landau level.

2.2. Aharanov-Bohm Phase

The Aharanov-Bohm effect can be observed in a system where a charged particle moves along a closed path along which no electromagnetic fields are present. However the corresponding vector potential $\hat{A}$ is not zero and there is some area enclosed by the path with a non zero magnetic field. When the particle moves along the path for one loop it picks up a relative phase leading to factor a $e^{i\phi}$ when compared to its original state. This phase factor can be computed as

$$e^{i\phi} = e^{\frac{i}{\hbar}\int_C q\hat{A}\mathrm{d}l}. \tag{7}$$

Here C denotes the contour of the path the particle takes. We can express the relative phase ϕ through the magnetic flux

$$\Phi_B = \int_C \hat{A}\mathrm{d}l \tag{8}$$

$$\phi = \frac{q}{\hbar}\Phi_B. \tag{9}$$

Note that the same phase factor is present even when the magnetic field along the path is not zero. For this reason we will refer to this phase as Aharanov-Bohm phase even though we do not have the classical setup of the Aharanov-Bohm experiment. One key difference we have to be mindful of is the fact that in the Aharanov-Bohm setup small changes of the path do not change the phase (small in the sense that the contour is deformed in way that the area on which the magnetic field is confined is still enclosed by the path in the same way). This path independence is lost when we drop the condition that the magnetic field has to be zero in proximity of the path.

2.3. Connection a Rotating Trap

An equivalent system can be realised using a rotating trap the goal of this chapter is to show that for a suitable choice of parameters the two system indeed produce Hamiltonians of the same form. In [1] a Bose-Einstein condensate consisting of ^{23}Na atoms is confined within a time-averaged orbiting potential trap. Within this setup the Bose-Einstein condensate was squeezed into a single Landau gauge wavefunction in the lowest Landau level.

In order to illustrate the connection between neutral particles in rotating traps and charged particles in a magnetic field we will looked at a simple version of a rotating trap. Consider a particle confined to xy-plane trapped inside a quadratic potential whilst the whole system is rotating around the z-axis. The Hamiltonian in this case can be written as

$$\hat{H} = \underbrace{\frac{p_x^2 + p_y^2}{2m}}_{\text{free particle}} + \underbrace{\frac{1}{2}m\omega^2(x^2+y^2)}_{\text{trap}} - \Omega(\underbrace{xp_y - yp_x}_{=L_z}), \tag{10}$$

by setting the two frequencies to the same value ($\omega = \Omega$) we get

$$\hat{H} = \frac{(p_x + m\omega y)^2}{2m} + \frac{(p_y - m\omega x)^2}{2m}. \tag{11}$$

This corresponds to the Hamiltonian of a charged particle in a magnetic field in symmetric gauge from equation (5). Now the following coordinates can be introduced

$$X = \frac{1}{2}(x + \frac{p_y}{m\omega}), \quad Y = \frac{1}{2}(y - \frac{p_x}{m\omega}) \qquad \text{(guiding center)} \tag{12}$$

$$\xi = \frac{1}{2}(x - \frac{p_y}{m\omega}) \quad \eta = \frac{1}{2}(y + \frac{p_x}{m\omega}) \qquad \text{(cyclotron)} \tag{13}$$

The original coordinates can be retrieved using $x = \xi + X$ and $y = \eta + Y$. It is important to keep in mind that unlike the original pairs of coordinates x,y (and p_x,p_y respectively) the new pairs of coordinates are not commuting $[X,Y] = -il_R^2$ and $[\xi,\eta] = il_R^2$. Here $l_R = \sqrt{\hbar/2m\omega}$ is the rotational equivalent of the magnetic length. The correspondence of the two systems is the following

$$2m\omega \leftrightarrow eB. \tag{14}$$

When looking at the new coordinates, we can interpret each pair as a pair of spatial and momentum coordinates. In new coordinates we get the Hamiltonian

$$\hat{H} = \hbar m\omega^2(\eta^2 + \xi^2) \tag{15}$$

which again has a similar form to the 1D harmonic oscillator Hamiltonian. This leads to energy levels similar to the Landau levels in the case of a charged particle. The Hamiltonian in (15) does not feature any guiding center coordinates. An important question which remains is how this transformation affects an additional potential $V(x,y)$ which is added to the Hamiltonian. This topic will we discussed in the next section.

2.4. Additional Potential in New Coordinates

A additional potential $V(x,y)$ transforms to $V(\xi + X,\eta + Y)$, in order to get an effective potential $\widetilde{V}(X,Y)$ we can project the potential onto the lowest energy Level with regards to the Hamiltonian in (15). The wave function corresponding to the lowest Level is

Gaussian shaped in the cyclotron coordinates η and ξ. Importantly it has to be noted that while for $V(x,y)$ the ordering of the the terms is irrelevant, the ordering of the terms in $\widetilde{V}(X,Y)$ can not be chosen arbitrarily since X and Y do not commutate. A general expression for a potential would be $V(x,y) = f(y)g(x)$, where g is a an analytic function with $g(x) = \sum_n a_n x^n$ in this case it is possible to rewrite the potential as

$$\sum_n \frac{a_n}{2^n} \sum_{k=0}^{n} \binom{n}{k} x^k f(y) x^{n-k} \tag{16}$$

When projecting to the lowest level the matrix elements can be written as

$$\begin{aligned}
&\left\langle X'\Psi_0 \,\middle|\, V(x,y) \,\middle|\, \Psi_0 X \right\rangle \\
&= \iint \mathrm{d}\xi \mathrm{d}\xi' \bar{\Psi}(\xi')\Psi(\xi) \sum_n \frac{a_n}{2^n} \sum_{k=0}^{n} \binom{n}{k} (X'+\xi')^k \iint \frac{\mathrm{d}\eta \mathrm{d}Y}{4\pi^2} e^{i(X'-X)Y} e^{-i(\xi'-\xi)\eta} f(Y+\eta)(X+\xi)^{n-k} \\
&= \iint \mathrm{d}\xi \mathrm{d}\xi' \bar{\Psi}(\xi')\Psi(\xi) g\left(\frac{X+X'+\xi+\xi'}{2}\right) \iint \frac{\mathrm{d}\eta \mathrm{d}Y}{4\pi^2} e^{i(X'-X)Y} e^{-i(\xi'-\xi)\eta} f(Y+\eta) \\
&\quad \text{with } R \coloneqq \frac{\xi+\xi'}{2} \text{ and } r \coloneqq \xi' - \xi \\
&= \int \frac{\mathrm{d}Y}{2\pi} e^{i(X'-X)Y} \underbrace{\int \mathrm{d}R \frac{1}{\sqrt{\pi l_R^2}} e^{\frac{-R^2}{l_R^2}} g\left(R + \frac{X+X'}{2}\right)}_{\coloneqq \widetilde{g}\left(\frac{X+X'}{2}\right)} \underbrace{\int \mathrm{d}\eta \frac{1}{\sqrt{\pi l_R^2}} f(Y+\eta) e^{\frac{-\eta^2}{l_R^2}}}_{\coloneqq \widetilde{f}(Y)} \\
&= \left\langle X' \middle| \widetilde{g}\left(\frac{X+X'}{2}\right) \widetilde{f}(Y) \middle| X \right\rangle
\end{aligned} \tag{17}$$

In (17) we can see that the effective potential can be calculated by convoluting f and g with a Gaussian. The magnetic length and its rotational equivalent represent a characteristic length scale in the system. Convolution with a Gaussian „smooths out“ the original function. This can lead to cases where $V(x,y)$ possesses a tunnel barrier which does not appear in $\widetilde{V}(X,Y)$. For example $V(x) = x^4 - x^2$ has two local minima and one local maximum in between, whereas in $\widetilde{V}(X,Y) = X^4 + 2X^2 + 1/4$ only one local minimum remains (for this example we have chosen $l_R = 1$). In contrast to this the convolution with a Gaussian can not create additional extrema (hence no additional tunnel barriers). For polynomials the leading coefficients stay the same and the corrections are again polynomials of lower degree. In order to obtain $\widetilde{V}(X,Y)$ from the corresponding $V(x,y)$ when the latter consists of polynomials one can use the following identity for Hermite polynomials.

$$\int_{-\infty}^{\infty} \mathrm{d}R \frac{H_n(x+R)}{2^n} \frac{e^{-R^2}}{\sqrt{\pi}} = x^n \tag{18}$$

The proof of this identity can be found in appendix A and can be generalized for arbitrary l_R by substituting accordingly. For any potential of the form $V(x,y) = A(x) + B(y)$ it is not necessary to pay closer attention to the ordering of the terms in the new coordinates. However as soon as mixed terms like xy are present the ordering does play a role which requires specific ordering rules to get the correct results. In [2] it is pointed out that when using the path integral (which we will do in later calculations) accepting Feynman's postulate that each path contributes proportional to its action is equivalent to applying Weyl's rule when constructing the quantum Hamiltonian. For this reason it is sensible

in our case to use Weyl Ordering. The issue of operator ordering when projecting onto the lowest Landau level is also addressed in [7]. It is fairly simple to Weyl order any polynomial terms using McCoy's formula

$$x^n y^m \to \frac{1}{2^n} \sum_{r=0}^{n} \binom{n}{r} X^r Y^m X^{n-r} \tag{19}$$

Given the fact that we intersted in a system with a potential which features trigonometric functions it is important to know how these functions transform when convoluted with a Gaussian. By looking at the integrals

$$\int_{-\infty}^{\infty} \mathrm{d}R \frac{\cos\left(b \cdot (R+x)\right)}{\sqrt{2\pi a}} \mathrm{e}^{-\frac{R^2}{2a}} = \cos\left(bx\right) \mathrm{e}^{-\frac{ab^2}{2}} \tag{20}$$

$$\int_{-\infty}^{\infty} \mathrm{d}R \frac{\sin\left(b \cdot (R+x)\right)}{\sqrt{2\pi a}} \mathrm{e}^{-\frac{R^2}{2a}} = \sin\left(bx\right) \mathrm{e}^{-\frac{ab^2}{2}} \tag{21}$$

it becomes obvious that for potentials of the form

$$V(x,y) = A\sin(\omega_1 x) + B\cos(\omega_2 x) + C\sin(\omega_3 y) + D\cos(\omega_4 y) \tag{22}$$

the effective potential has the same form and only its factors before the individual terms change.

Now a quick summary of the results in this chapter we found that a charged particle in a magnetic field can be forced into the lowest Landau level when the energy in the system is small and the magnetic field is large. Neutral particle in rotating traps can be used as an equivalent system where the correspondence is $2m\omega \leftrightarrow eB$. Additionally we saw that a charged particle moving along a closed loop through a magnetic field picks up a phase $\phi = q\Phi_B/\hbar$ which is proportional to the enclosed magnetic flux.

By introducing cyclotron and guiding center coordinates we get Landau Levels for the cyclotron coordinates. We can project an added potential onto the lowest Landau level by convolution with Gaussian without creating additional tunneling problems. The effective potential is function of the guiding center coordinates which do not commute.

3. Instantons in a Double Well Potential

In this chapter we introduce the instanton technique which will be used in chapter 4. We will explicitly calculate the tunnel probability for a double well potential which is a standard example for instanton calculations and will be a useful comparison to the tunneling probability calculated in later chapters. We first motivate the instanton approximation as an approximation around stationary paths. We begin calculating the instanton solutions and the corresponding instanton action. Then we compute the tunneling probability and use the euclidean path integral to calculate the partition function. A detailed overview of the instanton technique can be found in [8].

Before we start introducing the instanton formalism let us take a look at the integral

$$\int_a^b f(x)e^{-\alpha g(x)}\mathrm{d}x \tag{23}$$

For $\alpha \to \infty$ integrals of this type can be approximated using Laplace's method. If $g(x)$ has one strict minimum at x_0 and $f(x_0) \neq 0$ then integral can be approximated by

$$\int_a^b f(x)e^{-\alpha g(x)}\mathrm{d}x \approx \sqrt{\frac{2\pi}{\alpha|g''(x_0)|}} f(x_0)e^{-\alpha g(x_0)}. \tag{24}$$

This method can be extended as follows, when there are multiple minima we can approximate by summing over the contributions of the individual minima. Another trick is to deform the integration contour in the complex plane in such a way, that we find a suitable stationary point which lies along the new contour and then apply this method. In the instanton formalism similar arguments are used to argue that the path integral can be approximated by contributions of stationary paths for which the functional derivative of the action functional vanishes.

Now we will introduce the path integral formalism. For a detailed derivation of the path integral where it is also applied to this problem we refer to [3]. Using the Feynman path integral the propagator for a time-translationally invariant system can be written as

$$K(a,b,t) = \left\langle x = a \,\middle|\, e^{-\frac{i\hat{H}t}{\hbar}} \,\middle|\, x = b \right\rangle = \int \mathrm{d}[x(t)] e^{\frac{i}{\hbar}S[x]}. \tag{25}$$

Here we integrate over all paths, both classically allowed and not, which start at $x(0) = b$ and end at $x(t) = a$. Each path is weighted proportionally to its action $S[x(t)]$. The path integral is normalized using the path integral measure $\mathrm{d}[x(t)]$. By introducing imaginary time $\tau = it$ we can perform what is called a Wick-rotation this leads to the euclidean path integral with propagator

$$K_E(a,b,\tau) = \left\langle x = a \,\middle|\, e^{-\frac{\hat{H}\tau}{\hbar}} \,\middle|\, x = b \right\rangle = \int \mathrm{d}[x(\tau)] e^{-\frac{1}{\hbar}S_E[x]}. \tag{26}$$

The subscript E denotes the euclidean action. When comparing the two actions

$$S = \int \mathrm{d}t \left(\frac{1}{2}m\dot{x}^2 - V(x)\right) \qquad S_E = \int \mathrm{d}\tau \left(\frac{1}{2}m\dot{x}^2 + V(x)\right) \tag{27}$$

it becomes visible that in the euclidean path integral the potential receives the opposite sign.

(a) (b)

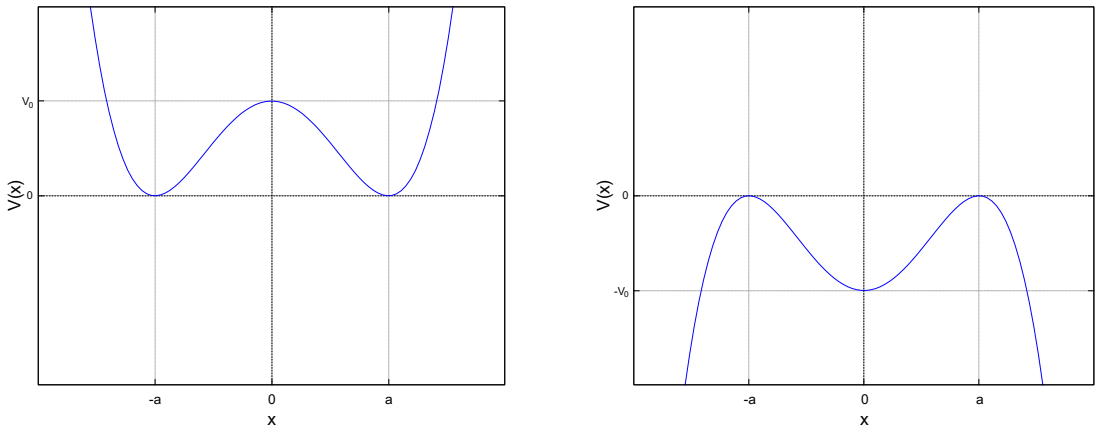

Figure 1: Depicted is the double well potential $V(x) = V_0(x^2 - a^2)^2$ and its inverted version on right.

The double well potential exhibits two minima separated by a tunnel barrier. Hence there is no classically allowed trajectory connecting both minima, assuming the energy in the system is lower than height the tunnel barrier. As a concrete Example we will consider the potential $V(x) = V_0(x^2 - a^2)^2$ pictured in 1. When changing the sign in front of the double well potential the two minima turn into maxima and there is a classically allowed trajectory between them. The potential features two minima turned maxima at $\pm a$ we will now proceed by calculating classical solutions for $\tilde{V} = -V(x)$ connecting the two points. Since $V(\pm a) = 0$ we have to set the total energy

$$E = T + \tilde{V} = 0. \tag{28}$$

T is the kinetic energy with derivatives taken with respect to τ

$$T = \frac{m}{2}\left(\frac{\mathrm{d}x}{\mathrm{d}\tau}\right)^2. \tag{29}$$

Taking the square root leads to the following differential equation

$$\frac{\mathrm{d}x}{\mathrm{d}\tau} = \pm\sqrt{\frac{2V(x)}{m}} = \pm\sqrt{\frac{2V_0}{m}}(a^2 - x^2). \tag{30}$$

Separation of variables leads to

$$\int_{x(\tau_0)}^{x(\tau)} \frac{\mathrm{d}x}{a^2 - x^2} = \pm\sqrt{\frac{2V_0}{m}} \int_{\tau_0}^{\tau} \mathrm{d}\tau \tag{31}$$

$$\left[\frac{1}{a}\mathrm{artanh}(x)\right]_{x(\tau_0)}^{x(\tau)} = \pm\sqrt{\frac{2V_0}{m}}(\tau - \tau_0) \tag{32}$$

We chose τ_0 in such a way that $x(\tau_0) = 0$. Then we can make use of the fact that tanh(x)

possesses the symmetry $\tanh(\pm x) = \pm\tanh(x)$ and obtain solutions of the form

$$x_{\text{inst}}(\tau) = \pm\tanh\left(a\sqrt{\frac{2V_0}{m}}(\tau - \tau_0)\right). \tag{33}$$

These solution are called instanton solutions, in a small area around τ_0 $x_{\text{inst}}(\tau)$ changes from being close to one minimum to being close to the other minimum. The sign in front of the instanton solution decides at which minima the solution starts and which it ends. Based on this a distinction can be made between instantons and anti-instantons.
Now we can continue by calculating the action for an instanton using equations (27) and (30) together with the fact that $E = 0$ along the instanton trajectory we get

$$\begin{aligned} S_{\text{inst}} &= \int_{-\infty}^{\infty} \mathrm{d}\tau\, m\left(\frac{\mathrm{d}x_{\text{inst}}}{\mathrm{d}\tau}\right)^2 && (34)\\ &= \int_{-a}^{a} \mathrm{d}x\, m\frac{\mathrm{d}x_{\text{inst}}}{\mathrm{d}\tau} && (35)\\ &= \int_{-a}^{a} \mathrm{d}x\, m\sqrt{\frac{2V_0}{m}}(a^2 - x^2) && (36)\\ &= \left[m\sqrt{\frac{2V_0}{m}}(a^2x - \frac{x^3}{3})\right]_{-a}^{a} && (37)\\ &= \sqrt{2V_0m}\frac{4}{3}a^3 && (38) \end{aligned}$$

For an anti-instanton the action is the same (in this case one would need to integrate from a to $-a$ which is compensated by the negative sign in front of the anti-instanton). The instanton action can now be used to approximate the tunneling probability $\mathcal{T}$ as follows

$$\mathcal{T} = |K_E(a, -a)|^2 \approx \exp\left(\frac{-2}{\hbar}S_{\text{inst}}\right) = \exp\left(\frac{-8\sqrt{2V_0m}a^3}{3\hbar}\right) \tag{39}$$

Now as we would expect equation (39) shows that $\mathcal{T}$ is exponentially decreased when increasing the height of the tunnel barrier through V_0 or its width by increasing a. In the next part we want to continue by approximating the partition function using the previously found instanton solution. Instead of restricting ourselves to single tunneling events, we can also look at cases where instanton are followed by anti instantons and so forth, now describing cases where we have tunneling back an forth through the tunnel barrier between the two wells. Trajectories starting and ending in the same well are described by n pairs of instantons and anti-instantons. The dilute gas approximation assumes that instantons and anti instanton are sufficiently separated in time making it is possible to treat them as a one dimensional non interacting gas. Using this approximation together with the fact that action is the same for instantons and anti-instantons we can write the action S_{2n} of n instanton anti-instanton pairs as

$$S_{2n} = 2nS_{\text{inst}}. \tag{40}$$

We should note that n is also allowed to be zero. In this case no tunneling takes place instead $x(\tau) = \pm a$ is constant and the action therefore is zero. Using the path integral

the partition function can be written as

$$Z = \mathrm{tr}\left(e^{-\beta\hat{H}/\hbar}\right) \tag{41}$$

$$= \int_{x(-\beta/2)=x(\beta/2)} \mathrm{d}[x(\tau)] e^{-\frac{1}{\hbar}\int_{-\beta/2}^{\beta} \mathrm{d}\tau\left(\frac{m}{2}\dot{x}^2+V(x)\right)} \tag{42}$$

Starting of we will first look at how the zero instanton configuration contributes to the path integral. We expand $x(\tau)$ around a as

$$x(\tau) = x_c(\tau) + \Delta x(\tau) \tag{43}$$

where $\Delta x(\tau)$ is assumed to be small and $\Delta x(\pm\beta/2) = 0$ and $x_c(\tau) = a$. Now we can expand $S[x(\tau)]$ in terms of δx as

$$S[x(\tau)] = S[x_c(\tau) + \Delta x(\tau)] \tag{44}$$

$$\begin{aligned} =& S[x_c(\tau)] + \int \mathrm{d}\tau \frac{\delta S[x_c]}{\delta \Delta x(\tau)} \Delta x(\tau) \\ &+ \frac{1}{2}\int\int \mathrm{d}\tau \mathrm{d}\tau' \frac{\delta^2 S[x_c]}{\delta\Delta x(\tau)\delta\Delta x(\tau')} \Delta x(\tau)\Delta x(\tau') + ... \end{aligned} \tag{45}$$

with $S[x_c] = 0$ and $\delta S[x_c]/\delta\Delta x(\tau) = 0$ we can approximate the zero instanton contribution (from $x_c(\tau) = a$) as

$$Z_0 \approx \int_{\Delta x(-\beta/2)=\Delta x(\beta/2)} \mathrm{d}[\Delta x(\tau)] e^{-\frac{1}{\hbar}\int_{-\beta/2}^{\beta} \mathrm{d}\tau\left(\frac{m}{2}(\dot{\Delta x})^2+\frac{1}{2}V''(x_c)(\Delta x)^2\right)} \tag{46}$$

$$= \int_{\Delta x(-\beta/2)=\Delta x(\beta/2)} \mathrm{d}[\Delta x(\tau)] e^{-\frac{1}{\hbar}\int_{-\beta/2}^{\beta} \mathrm{d}\tau\left(\frac{m}{2}(\dot{\Delta x})^2+\frac{1}{2}(8V_0a^2)(\Delta x)^2\right)}. \tag{47}$$

This expression is now the same as for the harmonic oscillator. By setting $V_0 = m\omega^2/8a^2$ we get

$$Z_0 = \sum_{n=0}^{\infty} e^{-\beta\hbar\omega(n+1/2)} \tag{48}$$

for $\beta \to \infty$ the $n = 0$ term in (48) dominates. Our next goal will be to express the instanton contributions of n pairs Z_{2n} through the zero and single instanton contributions Z_0 and Z_1. First we explicitly look at the $n = 1$, with the goal to later generalize this result to arbitrary n. We start by dividing the path integral into two regions, one where a instanton is present (I) and one where an anti-instanton is present (II). The subscripts

$1i$ and $1ai$ denote that an (anti-)instanton is present.

$$Z_2 = \int_{1i+1ai} \mathrm{d}[x(\tau)] e^{\frac{-1}{\hbar}\int_{-\beta/2}^{\beta/2} \mathrm{d}\tau L(x(\tau))} \tag{49}$$

$$= \int_{1i,\tau\in I} \mathrm{d}[x(\tau)] e^{\frac{-1}{\hbar}\int_I \mathrm{d}\tau L(x(\tau))} \int_{1ai,\tau\in II} \mathrm{d}[x(\tau)] e^{\frac{-1}{\hbar}\int_{II} \mathrm{d}\tau L(x(\tau))} \tag{50}$$

$$= \int_{1i,\tau\in I} \mathrm{d}[x(\tau)] e^{\frac{-1}{\hbar}\int_I \mathrm{d}\tau L(x(\tau))} \int_{0i,\tau\in II} \mathrm{d}[x(\tau)] e^{\frac{-1}{\hbar}\int_{II} \mathrm{d}\tau L(x(\tau))} \times$$

$$\int_{0i,\tau\in I} \mathrm{d}[x(\tau)] e^{\frac{-1}{\hbar}\int_I \mathrm{d}\tau L(x(\tau))} \int_{1i,\tau\in II} \mathrm{d}[x(\tau)] e^{\frac{-1}{\hbar}\int_{II} \mathrm{d}\tau L(x(\tau))} \times \tag{51}$$

$$\left(\int_{0i,\tau\in I} \mathrm{d}[x(\tau)] e^{\frac{-1}{\hbar}\int_I \mathrm{d}\tau L(x(\tau))} \int_{0i,\tau\in II} \mathrm{d}[x(\tau)] e^{\frac{-1}{\hbar}\int_{II} \mathrm{d}\tau L(x(\tau))}\right)^{-1}$$

Here we have made use of the fact that the path integral factorizes. Keep in mind that we imposed the restriction that the instanton proceeds the anti-instanton, in order to remove this restriction we have to divide the terms in (51) by 2. This leads to

$$Z_2 = \frac{1}{2}\frac{Z_1^2}{Z_0} = \frac{1}{2}R^2 Z_0 \tag{52}$$

where Z_1 is the single instanton contribution and R is the ratio

$$R = \frac{Z_1}{Z_0}. \tag{53}$$

Now to generalize this result for general n we have to divide into $2n$ regions instead of two. There are $(2n)!$ ways to order the (anti-)instantons, instead of dividing by two we now have to divide by $(2n)!$. Equation (52) generalizes to

$$Z_2 = \frac{1}{(2n)!}\frac{Z_1^{2n}}{Z_0^{2n-1}} = \frac{1}{(2n)!}R^{2n} Z_0. \tag{54}$$

Using the results from (54) it is possible to express the partition function as

$$Z(\beta) = \sum_{n=0}^{\infty} Z_{2n} \tag{55}$$

$$= Z_0 \sum_{n=1}^{\infty} \frac{1}{(2n)!} R^{2n} Z_0 \tag{56}$$

$$= Z_0 \cosh(R) \xrightarrow{\beta\to\infty} e^{-\frac{\hbar\beta\omega}{2}+R} \tag{57}$$

Here we made use of equation (48) and the fact that $R \propto \beta$. The lowest energy level of a double well where no tunneling is possible is degenerate, but by introducing tunneling the degeneracy is lifted and the energy of the symmetric/ anti-symmetric ground state are shifted. The symmetric state now being energetically lower than anti-symmetric one. The ground state energy can be written as

$$E_0 = \frac{\hbar\omega}{2} + \epsilon \tag{58}$$

where ϵ is the energy shift due to tunneling, which can be derived from (57) as

$$\epsilon = \lim_{\beta \to \infty} \left(-\frac{R}{\beta} \right) \tag{59}$$

To obtain R we have to calculate the quotient of two functional determinants. This is a lengthy calculation which we will not carry out. It is similar to the one done later in section 4.3. The corresponding calculation for the double well in full detail can be found in [10].

In this chapter we have familiarized ourselves with the instanton formalism and the dilute gas approximation. We found instanton and anti-instanton solutions and their respective instanton action. The Tunneling probability was computed showing and exponential decrease for increasing height $V_0 a^2$ and width $2a$ of the tunnel barrier.

4. Instantons for a Periodic Hamiltonian

In this chapter take a look at the case where we have $\hat{H} = 2 - \cos(x) - \cos(y)$. We treat this as a one dimensional Hamiltonian with a non classical kinetic energy term. We start by looking at equipotential lines which connect two neighbouring minima. In order to find equipotential lines we allow one of the coordinates to be complex. Then we solve the Euler-Lagrange equations and find instanton solutions connected to nearest neighbour tunneling in the $\pm x$ and $\pm y$-direction. We discuss how rescaling the coordinates as well as the potential influence the instanton solutions and their respective action. In section 4.3 we closely follow calculations from [5] where the partition function is computed from which energy corrections to the ground state can be derived. We conclude by discussing the energy spectrum (Hofstadter Butterfly [9]) and showing that the path dependent tunneling phases can be identified as the Aharanov-Bohm phase.

4.1. Finding Instanton Solutions

The Hamiltonian of our interest is

$$\hat{H}(x,y) = 2 - \cos(x) - \cos(y) \tag{60}$$

where x,y possess the same commutator $[x,y] = il_B^2$ as X,Y in chapter 2. This allows us to interpret one of the variables as a spacial coordinate and the other coordinate as momentum. We can approach the system as a quasi one dimensional. Instanton calculations for this Hamiltonian where already made in [5] and [6]. The energy of the Hamiltonian in (60) is minimal when both x and y are multiples of 2π. In those cases we get $\hat{H}(2\pi n_x,2\pi n_y) = 0$ as seen in figure 2a. The minima form a square lattice with lattice constant 2π. The instanton solutions we are interested in are those connecting two neighboring minima.

(a) (b)

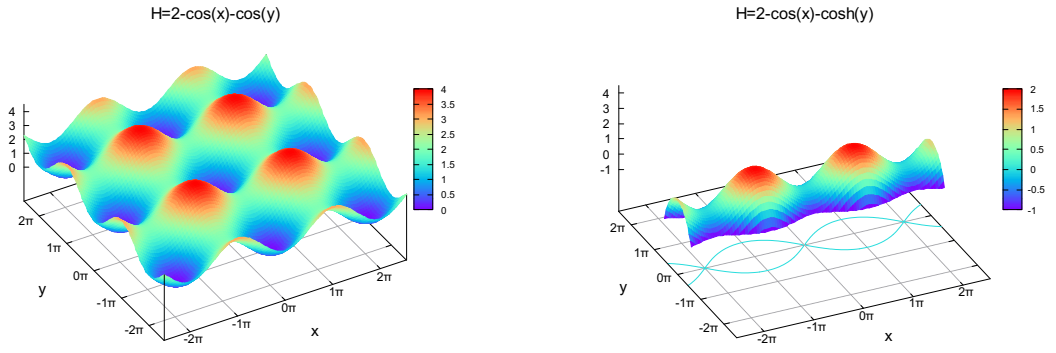

Figure 2: Depicted are the Hamiltonians $2 - \cos(x) - \cos(y)$ on left and $2 - \cos(x) - \cosh(y)$ on the right. The line under the graph on the right-hand side shows the equipotential line where $H(x,y) = 0$.

Looking at figure 2a it immediately becomes clear that there are no equipotential lines connecting two neighbouring minima. However when replacing one of the variables for example y as purely imaginary the Hamiltonian transforms to $\hat{H} = 2 - \cos(x) - \cosh(y)$

as depicted in figure 2b and in this case there clearly are some equipotential lines connecting some of the minima. In order two find the instanton trajectories connected to those equipotential lines we start by formulating the Euler-Lagrange equations for the Hamiltonian given in (60).

When interpreting y as the momentum canonically conjugate to x it is important to take into consideration that there is no classical kinetic energy $y^2/(2m)$ but instead a $\cos(y)$ term in the Hamiltonian. In the euclidean path integral each path is weighted by the factor

$$\exp\left(\frac{-1}{\hbar}\int_{\tau_a}^{\tau_b} \mathrm{d}\tau[h(p(\tau),q(\tau)) - ip(\tau)\dot{q(\tau)}]\right) \tag{61}$$

where $h(p,q)$ is the Weyl transform of $\hat{H}(\hat{P},\hat{Q})$ since the Hamiltonian in our case has no mixed terms the question of operator ordering is not relevant. l_B^2 plays the role of $\hbar$ when considering neutral particles in a rotating trap we just have to replace l_B^2 by l_R^2. Note using instanton approximations we usually use the fact that $\hbar \ll 1$ now that we replaced $\hbar$ we instead have to demand that $l_B^2 \ll 1$. In the case $l_B^2 \gg 1$ we could rescale all coordinates by a factor $1/l_B^2$ and then proceed in those coordinates. We will not pursue this case further instead we stay with case where $l_B^2 \ll 1$, which is the case for large magnetic fields.
Choosing y as momentum the factor in the path integral from (61) changes into

$$\exp\left(\frac{-1}{l_B^2}\int_{\tau_a}^{\tau_b} \mathrm{d}\tau[h(x(\tau),y(\tau)) - iy(\tau)\dot{x(\tau)}]\right) \tag{62}$$

This way we can formulate the corresponding Lagrangian L as

$$L = 2 - \cos(x) - \cos(y) - i\dot{x}y \tag{63}$$
$$\tag{64}$$

from which the following Euler-Lagrange equations arise:

$$-i\dot{y} = \sin(x) \tag{65}$$
$$i\dot{x} = \sin(y), \tag{66}$$

When both x and y are resticted to being real only trivial constant solutions exist to the equations (65) and (66).In our case by allowing one of the variables to be complex we can find the desired instanton solutions. It should be noted that for some Hamiltonians both variables have to be complex.

Since the instanton solution (x_i,y_i) should connect two minima we additionally impose the restriction $\hat{H}((x_i,y_i) = 0$ or equivalently

$$\cos(x_i) + \cos(y_i) = 2 \tag{67}$$

Using equation (66) y_i can be eliminated. Manipulating the terms and squaring both sides than leads to

$$1 + \dot{x}_i^2 = (2 - \cos(x_i))^2. \tag{68}$$

The substitution $u = \cos(x_i/2)$ allows us to get rid of trigonometric functions and leaves

us with

$$\dot{u}^2 = 2 - 5u^2 + 4u^4 - u^6 \tag{69}$$

Using $w^2 = 1/(2/u^2 - 1)$ the equation simplifies to

$$\dot{w}^2 = (1 - w^2)^2 \tag{70}$$

In Order to solve equation (70) it is sufficient to find a solution which satisfies the equation without the square on both sides. This can be done by separation of variables. Using

$$\int \frac{\mathrm{d}w}{1 - w^2} = \operatorname{artanh}(w) + C \qquad (\text{for} - 1 < w < 1) \tag{71}$$

we get the $w(t) = \tanh(t)$ as a solution of $\dot{w} = 1 - w^2$. By re-substituting the variables back to x_i and making use of the fact that (65) and (66) are both autonomous the instanton solution

$$x_i(\tau) = 2 \arccos\left(-\frac{\sqrt{2}\tanh(\tau - \tau_0)}{\sqrt{1 + \tanh^2(\tau - \tau_0)}}\right). \tag{72}$$

is obtained. With the help of equation (67) its possible to calculate y_i.

$$y_i(\tau) = \arccos(2 - \cos(x_i)) \tag{73}$$

$$\overset{(72)}{=} \arccos\left(1 + \frac{2}{\cosh(2(\tau - \tau_0))}\right) \tag{74}$$

The Argument in the arccos is always greater than 1 therefore $y_i(t)$ is complex. Both the x and y trajectories are plotted in figure 3. For $\tau \to -\infty$ x_i and y_i approach 0, for $\tau \to \infty$ x_i approaches 2π and y_i strives towards 0.

(a) (b)

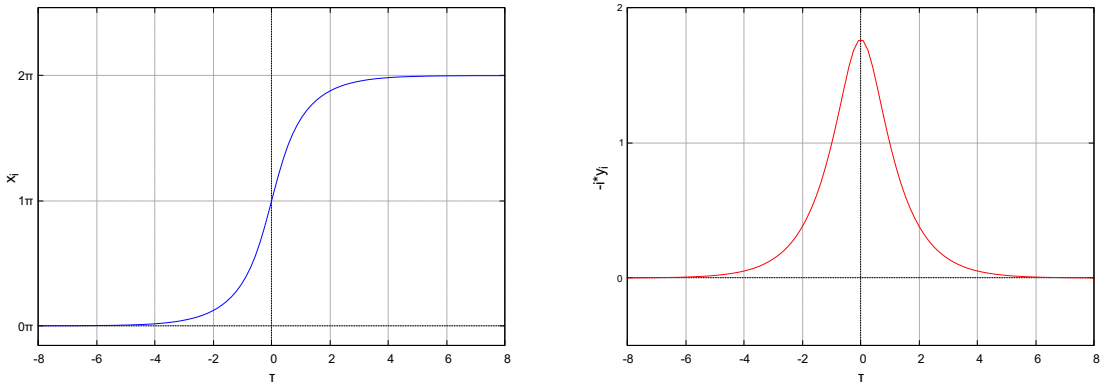

Figure 3: Depicted are $x_i(\tau)$ and $-i \cdot y_i(\tau)$ for the x-instanton starting at (0,0) with $\tau_0 = 0$.

These instanton solutions are not unique solutions, it is possible to shift x_i and y_i by $2\pi n_x$ and $2\pi n_y$ respectively. This follows from the periodicity of the Hamiltonian and demonstrates that instead of starting at (0,0) and tunneling to $(2\pi,)$ we can also start

at $(2\pi n_x,2\pi n_y)$ then the instanton describes tunneling to $(2\pi(n_x+1),2\pi n_y)$. We can also tunnel in the opposite direction, the anti-instantons connected to this are given by (-x_i,-y_i). Due to $\cos(-x) = \cos(x)$ and $\sin(-x) = -\sin(x)$ together with the fact that (x_i,y_i) fulfill (65), (66) and (67) it follows that the anti-instantons also fulfill those equations. Anti-instantons describe the tunneling events $(2\pi n_x,2\pi n_y) \to (2\pi(n_x-1),2\pi n_y)$. Up until now all the instantons describe tunneling along the x-axis we will call them x-instantons. There is a second type of instantons y-instantons which are related to tunneling events along the y-axis. In order to obtain them y has to be chosen to be real and x as complex. It is not necessary to repeat all of the calculations above instead we can use the symmetry of the Euler-Lagrange equations. This leads to y-instantons given by $(-y_i,x_i)$. To recap we have now constructed 4 types of instantons one for each spatial direction.

The x-instanton

$$x(\tau) = x_i(\tau) + 2\pi n_x\,, \quad y(\tau) = y_i(\tau) + 2\pi n_y \tag{75}$$

The x-anti-instanton

$$x(\tau) = -x_i(\tau) + 2\pi n_x\,, \quad y(\tau) = -y_i(\tau) + 2\pi n_y \tag{76}$$

The y-instanton

$$x(\tau) = -y_i(\tau) + 2\pi n_x\,, \quad y(\tau) = x_i(\tau) + 2\pi n_y \tag{77}$$

The y-anti-instanton

$$x(\tau) = y_i(\tau) + 2\pi n_x\,, \quad y(\tau) = -x_i(\tau) + 2\pi n_y \tag{78}$$

For a short moment we will consider the more general Hamiltonian

$$\hat{H} = V_0(2 - \cos(x/a) - \cos(y/a)) \tag{79}$$

Which leads to the slightly modified Euler-Lagrange equations

$$-i\dot{y} = \frac{V_0}{a}\sin(x/a) \tag{80}$$

$$i\dot{x} = \frac{V_0}{a}\sin(y/a), \tag{81}$$

The solutions to those equation can be constructed from the instanton solution we just found. The new instanton solutions are given by $(x_I,y_I) = (ax_i(V_0\tau/a^2),ay_i(V_0\tau/a^2))$. It is easy to check that they also satisfy

$$V_0(2 - \cos(x_I/a) - \cos(y_I/a)) = 0. \tag{82}$$

4.2. Calculating the Instanton Action

To calculate the instanton action the exact form of the instanton is not needed, equation (67) together with knowing the start and end points is sufficient. For the x-instanton

starting at the origin we get

$$\begin{aligned}
S_i =& \int_{-\infty}^{\infty} \mathrm{d}\tau V_0 \underbrace{(2-\cos(x_I/a)-\cos(y_I/a))}_{=0} - i\dot{x_I}y_I \\
=& -i\int_0^{2\pi a} y_I(x_I)\mathrm{d}x_i \\
\overset{(82)}{=}& -i\int_0^{2\pi a} a\cdot\arccos(2-\cos(x_I))\mathrm{d}x_I \\
=& -ia^2\int_0^{2\pi}\cdot\arccos(2-\cos(v))\mathrm{d}v \\
=& 2a^2\int_0^{\pi}\operatorname{arcosh}(2-\cos(v))\mathrm{d}v \\
=& 2a^2\int_0^{\pi}\operatorname{arcosh}(1+\sin^2(v/2))\mathrm{d}v \\
=& 4a^2\int_0^{\pi}\operatorname{arsinh}(\sin(v/2))\mathrm{d}v \\
=& 8a^2\int_0^{1}\frac{\operatorname{arsinh}(u)}{1-u^2}\mathrm{d}u \\
=& 8a^2G
\end{aligned} \tag{83}$$

Here we used the identity $2\mathrm{arsinh}(x) = \mathrm{arcosh}(1+x^2)$ and afterwards substituted $u = \sin(v/2)$. What we are left with is an integral representation of the Catalan's constant $G \approx 0{,}916$. This result is in agreement with the instanton actions calculated in [5] and [6]. Remarkably $S_i$does not depend on V_0. The reason for this is that V_0 does not appear in $y_I(x_I)$ which is due to the fact that V_0 does not impact the trajectory shown in figure 2. For general n_x,n_y we get

$$S_{x^+} = -i\int_{2\pi a n_x}^{2\pi a(n_x+1)} y_I(x_I) + 2\pi a n_y \mathrm{d}x_I \tag{84}$$

$$= 8a^2G - i4\pi^2a^2n_y \tag{85}$$

with same calculation for the x-anti-instanton leading to $S_{x^-} = 8a^2G + i4\pi^2a^2n_y$. For the y-instantons we can repeat these steps.

$$S_{y^+} = -\int_{-\infty}^{\infty}\mathrm{d}\tau i\dot{x_i}y_i \tag{86}$$

$$= -i\left[x_Iy_I\right]_{-\infty}^{\infty} + i\int_{-\infty}^{\infty}\mathrm{d}\tau i\dot{y_I}x_I \tag{87}$$

$$= -ia^2(2\pi n_x 2\pi(n_y+1) - 2\pi n_x 2\pi n_y) + i\int_{2\pi a n_y}^{2\pi a(n_y+1)} x_I(y_I) + 2\pi a n_x \mathrm{d}y_I \tag{88}$$

$$= -i4\pi^2a^2n_x + 8a^2G + i4\pi^2a^2n_x = 8a^2G \tag{89}$$

For the y-anti-instantons the same calculations lead to $S_{y^-} = 8a^2G$. Unlike $S_{x^\pm}$ the action for the y-(anti-)instantons has no imaginary part and n_x does not contribute to the action. This raises questions the terms in the Hamiltonian featuring x and those featuring y are the same. This can be explained by the fact that we choose one as spatial coordinate and the other as the conjugated momentum, essentially choosing a gauge which should bear no explicit measurable consequences.

The imaginary part of the action is related to a phase which is picked when tunneling and is rooted in the fact that x and y do not commutate. The exact influence of those phases will be discussed in section 4.4 The tunneling probability can be approximated as

$$\mathcal{T} \approx \exp\left(\frac{-2}{l_B^2}\mathrm{Re}(S_i)\right) = \exp\left(\frac{-2eB}{\hbar}a^2 8G\right) = \exp\left(\frac{-16e}{\hbar}\Phi_B G\right) \tag{90}$$

The tunneling probability does not depend on V_0, this a clear difference to what we would normally expect. Namely an exponential decay with the height of tunnel barrier. In later chapters we will use the tunneling rate

$$J \approx \exp\left(\frac{-8e}{\hbar}\Phi_B G\right). \tag{91}$$

4.3. Energy Corrections due to Tunneling

Returning back to the unmodified Hamiltonian we can take a look at the energy corrections due to tunneling. The partition function in the euclidean path integral formalism can be written as

$$Z(\beta) = \iint \mathcal{D}[x]\mathcal{D}[y] e^{-\frac{1}{l_B^2}\int_{-\beta/2}^{\beta/2}.\mathrm{d}\tau(h(x,y)-i\dot{x}y)}. \tag{92}$$

As already mentioned l_B^2 plays the role of $\hbar$, additionally the integral of the momentum variable y has not been carried out yet. This is due to the fact that y does not appear as a quadratic term as would be the case for Hamiltonians with standard kinetic energy. In order to calculate the one instanton contribution to the partition function, we can expand around the instanton solutions as follows $x = x_i + \delta x$ and $y = y_i + \delta y$. We assume the deviations from the instanton solution δx and δy to be small and $\delta x(\pm\beta/2) = \delta y(\pm\beta/2) = 0$. This way equation (92) becomes

$$Z_1(\beta) = \iint \mathcal{D}[\delta x]\mathcal{D}[\delta y] e^{-\frac{1}{l_B^2}\int_{-\beta/2}^{\beta/2}\mathrm{d}\tau(2-\cos(x_i+\delta x)-\cos(y_i+\delta y)-i(\dot{x_i}+\dot{\delta x})(y_i+\delta y))} \tag{93}$$

Looking at the integrand we have

$$\begin{aligned}
&2-\cos(x_i+\delta x)-\cos(y_i+\delta y)-i(\dot{x_i}+\dot{\delta x})(y_i+\delta y)) && (94)\\
=&2-\cos(x_i)\cos(\delta x)+\sin(x_i)\sin(\delta x)-\cos(y_i)\cos(\delta y)+\sin(y_i)\sin(\delta y)\\
&-i\dot{x_i}y_i-i\dot{\delta x}y_i-i\dot{x_i}y_i-i\dot{\delta x}\delta y && (95)\\
\approx&2-\cos(x_i)(1-\delta x^2/2)-i\dot{y_i}\delta x-\cos(y_i)(1-\delta y^2/2)+i\dot{x_i}\delta y-i\dot{x_i}y_i\\
&-i\dot{\delta x}y_i-i\dot{x_i}\delta y-i\dot{\delta x}\delta y && (96)\\
=&(2-\cos(x_i)-cos(y_i)-i\dot{x_i}y_i)+(\cos(x_i)\delta x^2/2+\cos(y_i)\delta y^2/2\\
&-i\dot{\delta x}\delta y)-(i\delta x\dot{y_i}+i\dot{\delta x}y_i) && (97)
\end{aligned}$$

Here we used approximated the δx and δy using $\sin(x) \approx x$ and $\cos(x) \approx 1 - x^2/2$. In addition we used the Euler-Lagrange equations (65) and (66) to further simplify. In (97) we are left with are three terms the first term is $h(x_i,y_i) - i\dot{x_i}y_i$, the second is quadratic in $\delta x, \delta y$ and the last term is the derivative of $i\delta x y_i$. The last terms vanishes when integrated out since $\delta x(\pm\beta/2) = 0$ and y_i is bounded. When integrated the first term yields the instanton action S_i.

This leaves us with

$$Z_1(\beta) \approx e^{-\frac{S_i}{l_B^2}+i\theta} \iint \mathcal{D}[\delta x]\mathcal{D}[\delta y] e^{-\frac{1}{2l_B^2}\int_{-\beta/2}^{\beta/2} \mathrm{d}\tau(\cos(x_i)\delta x^2+\cos(y_i)\delta y^2-2i\dot{\delta}x\delta y)} \tag{98}$$

The Bloch angle θ introduced in this equation stems from eigenvalues/eigenstates of the translation operator.There are two Bloch angles θ_x,θ_y which depend on the instanton we are looking at. For anti-instanton the sign is negative. They dictate where a state lays within the bands in the energy spectrum of the Hofstadter butterfly, and are discussed in more detail in [duan]. We will not concern us further with these angles since they do not contribute to closed tunneling paths.

As a next step we introduce $\delta\tilde{y} = \sqrt{\cos(y_i)}\delta y$ and $\delta\tilde{x} = \delta x/\sqrt{\cos(y_i)}$ making use of the fact that $\mathcal{D}[\delta x]\mathcal{D}[\delta y] = \mathcal{D}[\delta\tilde{x}]\mathcal{D}[\delta\tilde{y}]$ we obtain

$$Z_1(\beta) \approx e^{-\frac{S_i}{l_B^2}+i\theta} \iint \mathcal{D}[\delta x]\mathcal{D}[\delta y] e^{-\frac{1}{2l_B^2}\int_{-\beta/2}^{\beta/2} \mathrm{d}\tau\cos(x_i)\cos(y_i)\delta\tilde{x}^2+\delta\tilde{y}^2-2i\partial_\tau(\sqrt{\cos(y_i)}\delta\tilde{x})\frac{\delta\tilde{y}}{\sqrt{\cos(y_i)}}} \tag{99}$$

$$= e^{-\frac{S_i}{l_B^2}+i\theta} \iint \mathcal{D}[\delta x] e^{-\frac{1}{2l_B^2}\int_{-\beta/2}^{\beta/2} \mathrm{d}\tau\frac{\partial_\tau(\delta\tilde{x}\sqrt{\cos(y_i)})^2}{\cos(y_i)}+\cos(y_i)\cos(x_i)\delta\tilde{x}^2} \tag{100}$$

$$= e^{-\frac{S_i}{l_B^2}+i\theta} \frac{1}{\sqrt{\det(\widetilde{O})}} \tag{101}$$

Where $\widetilde{O}$ is the operator $\widetilde{O} = -\sqrt{\cos(y_i)}\partial_\tau(1/\cos(y_i))\partial_t\sqrt{\cos(y_i)}+\cos(y_i)\cos(x_i)$. When dealing with functional determinants it is important to check whether the operator possesses a zero mode, meaning an eigenstate with eigenvalue 0. With the help of the Euler-Lagrange equations we see that

$$\widetilde{O}\Psi_0 = \widetilde{O}\frac{\dot{x}_i}{\sqrt{\cos(y_i)}} = 0. \tag{102}$$

$\widetilde{O}$ therefore has a zero mode Ψ_0 which has to be treated separately. In order to this the we consider the operator $\widetilde{O}+\lambda$ where the eigenvalue of the zero mode now becomes λ and can be separated. In the end this leads to

$$Z_1(\beta) \approx e^{-\frac{S_i}{l_B^2}+i\theta} \frac{\mu\beta}{\sqrt{\det'(\widetilde{O})}} \tag{103}$$

where $\mu = \sqrt{N^2/(2\pi\Phi)}$ and N is the normalization constant of Ψ_0. The primed functionaldeterminant signals that the zero mode was excluded.

For Z_0 expanding around a constant solution of the Euler-Lagrange equations directly leads to

$$Z_0(\beta) = \frac{1}{\sqrt{\det(O_0}} \tag{104}$$

with the operator $O_0 = -\partial_t a u^2 + 1$. The dilute instanton gas approximation can now be used to calculate the partition function only using Z_{-1}, Z_0 and Z_1 for which we just

found suitable expressions. The partition function can be rewritten as follows

$$Z(\beta) = \sum_{k\in\mathbb{Z}} Z_k = Z_0 \left(\sum_{k\in\mathbb{Z}} \hat{Z}_k \right) \qquad \text{with} \quad \hat{Z}_k = \frac{Z_k}{Z_0} \tag{105}$$

$$\hat{Z}_k \approx \sum_{n-\widetilde{n}=k} \frac{\hat{Z}_1}{n!} \frac{\hat{Z_{-1}}}{\widetilde{n}!}. \tag{106}$$

Plugging (106) in equation (105) yields

$$Z(\beta) \approx Z_0 e^{\hat{Z}_1 + \hat{Z}_{-1}}. \tag{107}$$

$\hat{Z}_1$ can be calculated using (104) and (103) the calculations concerning the quotient of the functional determinants can be found in [5]. The method used for this can be found in appendix B .

$$\hat{Z}_{\pm 1} = e^{-\frac{S_i}{l_B^2} \pm i\theta} \mu\beta \sqrt{\frac{\det(O_0)}{\det'(\widetilde{O})}} \tag{108}$$

$$\approx e^{-\frac{S_i}{l_B^2} \pm i\theta} \frac{4\beta}{\sqrt{2\pi} l_B} \tag{109}$$

The partition function then takes the shape

$$Z = C e^{-\frac{\beta}{l_B^2} \left(E_0 + 8 \frac{l_B}{\sqrt{2\pi}} \cos(\theta) e^{-\frac{S_i}{l_B^2}} \right)} \tag{110}$$

Since there are actually two types of instanton we have to consider both θ_x and θ_y the resulting energy corrections can be derived from (110) as

$$\Delta E_x = 8\sqrt{\frac{l_B^2}{2\pi}} \cos(\theta_x) e^{-\frac{S_i}{l_B^2}} \qquad \text{und} \qquad \Delta E_y = 8\sqrt{\frac{l_B^2}{2\pi}} \cos(\theta_y) e^{-\frac{S_i}{l_B^2}}. \tag{111}$$

The so-called Hofstadter butterfly refers to energy spectrum of this system and is depicted in figure 4. It was originally discussed by Hofstadter in [9] and shows a self similar structure. The Bloch angles determine were within a band a state lies energetically speaking. Φ in figure 4 case refers to the magnetic flux trough a unit cell. For rational $\Phi/2\pi = p/q$ there are q different energy bands present. Note that for $\Phi/2\pi = 1/2$ the two bands touch each other at $E = 2$ so that it seems like there is only one band present.

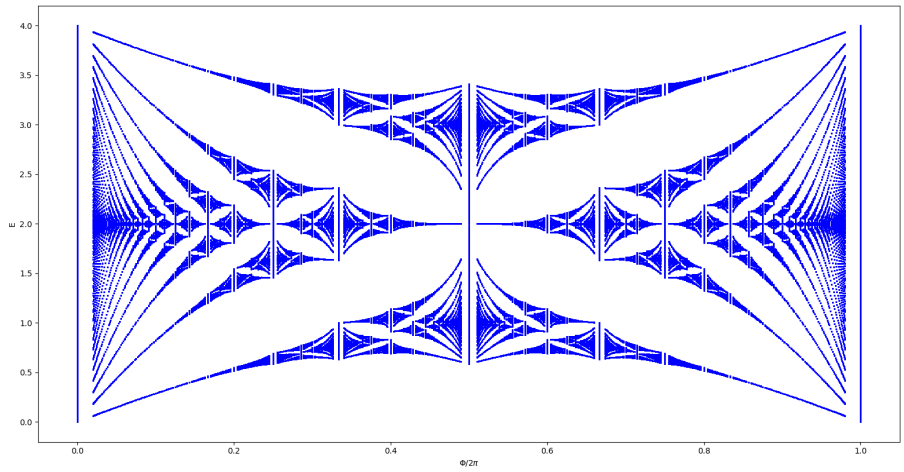

Figure 4: Hoftstadter Butterfly energy spectrum as a function of $\Phi/2\pi$ plotted are values for $\Phi/2\pi = p/q$ with $p \leq q \leq 50$.

Figure 4 was created by numerically solving for the Eigenvalues of the $q \times q$ Hamiltonian taken from [5] with matrix elements

$$\hat{H}i,j(k_x,k_y) = \begin{cases} 2 - \cos\left(k_x + 2\pi jp/q\right) & i = j \\ -e^{k_y}/2 & |i-j| = 1 \vee |i-j| = q-1 \\ 0 & \text{else .} \end{cases} \tag{112}$$

4.4. Phases Introduced Through Tunneling

We begin with a short remark concerning the Bloch angles. For $l_B^2 = \frac{2\pi}{q}$ with $q \in \mathbb{N}$ there are simultaneous eigenstates of

$$\widetilde{T}_y = e^{i\frac{2\pi x}{l_B^2}}, \quad \widetilde{T}_x = e^{-i\frac{2\pi y}{l_B^2}} \tag{113}$$

with eigenvalues

$$\widetilde{T}_x \left|\Psi\right\rangle = e^{i\theta_x} \left|\Psi\right\rangle, \quad \widetilde{T}_y \left|\Psi\right\rangle = e^{i\theta_y} \left|\Psi\right\rangle \tag{114}$$

The inverse operators are connected to anti-instantons and produce Bloch angles $-\theta_x and -\theta_y$. Bloch angles introduce phases while tunneling which are not path dependent and therefore only add a local phase which has no relevance when investigating how different paths with same start and end points interfere. The phase caused by the magnetic flux trough the lattice cells is path dependent and caused by the fact that we have

$$\widetilde{T}_x\widetilde{T}_y = e^{-i\frac{4\pi^2}{l_B^2}} \widetilde{T}_y\widetilde{T}_x. \tag{115}$$

If we recall the imaginary part of the instanton action of the x-instanton we have

$$-\mathrm{Im}(S_{x^+})/l_B^2 = a^2 \frac{eB}{\hbar} 4\pi^2 n_y \tag{116}$$

An easy case to consider would be the following, we start with a x-instanton at $n_y = 0$ followed by a y-instanton both add no phase then a x-anti-instanton which adds the phase $-4\pi^2 a^2(eB)/\hbar$ and finally a y-anti-instanton which allows adds no phase. From the Bloch angles we get no contribution ($\theta_x + \theta_y - \theta_x - \theta_y = 0$). The size of the unit cell is given by $A = (2\pi a)^2$ the magnetic flux through the unit cell is then given by

$$\Phi_0 = BA = 4\pi^2 B a^2. \tag{117}$$

The Aharonov–Bohm effect predicts the phase

$$\phi_0 = \frac{q}{\hbar}\Phi_0 = \frac{-e}{\hbar} 4\pi^2 B a^2 \tag{118}$$

which allows us to identify the phase related to the imaginary part of S_i with the Aharanov-Bohm phase from section 2.2.
In figure 5 we show an example for a more complicated path which illustrates that the phase is proportional to magnetic flux trough the area enclosed by the path for all arbitrary closed paths (still with the restriction that we only consider tunneling to the nearest neighbors). The exact phases along one tunnel path depend on our choice for the origin where $n_x = n_y = 0$, but for a closed path shifting the entire path in one direction does not result in a change of the total phase. In figure 5 there are four cells which are enclosed in a way that the path around them is traversed in mathematically positive direction and one cell where the path around it is traversed in mathematically negative direction. For this reason the resulting total phase is $3\Phi_0$ instead of $5\Phi_0$.

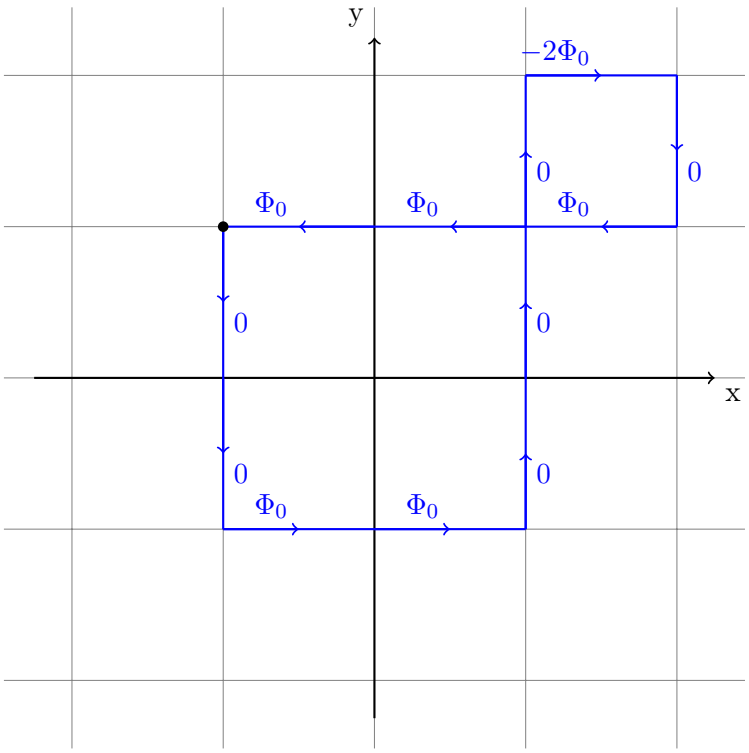

Figure 5: The graphic displays an exemplary path and the phases which get picked up on its way.

In this chapter we determined the complex instanton solutions and calculated the real part of the instanton action as $\mathrm{Re}(S_i) = 8a^2G$. Additionally we were able to identify the imaginary part of the instanton action with the Aharanov-Bohm phase. We found that a prefactor V_0 in front of the Hamiltonian does not appear in the instanton action and therefore we get a tunneling probability which does not depend on V_0. We should mention here that in the limit $V_0 \to 0$ the instanton approximation is not valid.

5. Time Evolution of a Particle on a Square Lattice

In the second part of this thesis we will investigate the question of how a particle will spread on a square lattice when tunneling induces the previously calculated phases. This chapter is split into two parts in the first we use the formalism of second quantization to calculate the time evolution of a state which is localized at t=0. We start by considering the linear chain and then extend this result to two dimensions for a square lattice. We start by diagonalizing the Hamiltonians in Fourier space and then compute the time evolution explicitly which leads to probability amplitudes given by Bessel functions. When introducing the previously calculated phases we can no longer diagonalize the Hamiltonian. For the case were no lattice is present we compute the time evolution of a free particle starting as Gaussian wave packet. The second part of this chapter consists of numerical analysis of the same systems we use continuous quantum random walks to obtain a probability distribution for a particle spreading across a finite square lattice. We check that the analytical and numerical results are consistent. After assessing the magnitude of potential finite size effects we investigate how the magnetic phase influences the speed with which a state can spreads across the lattice.

5.1. Analytical Approach Using Second Quantization

We start by writing down the Hamiltonian for a one dimensional chain where only nearest neighbor tunneling is allowed using second quantization.

$$\hat{H} = \sum_{n\in\mathbb{Z}} \epsilon \hat{c}_n^\dagger \hat{c}_n - J\left(\hat{c}_n^\dagger \hat{c}_{n+1} + \hat{c}_{n+1}^\dagger \hat{c}_n\right) \tag{119}$$

Here $\hat{c}_n^\dagger$ and $\hat{c}_n$ are the creation/annihilation operators creating/removing a particle at the lattice site n. Here we assume a constant tunnel rate J with no additional phases being introduced by tunneling. Our approach to diagonalize this Hamiltonian will involve the use Fourier transformation which is not surprising given the periodicity of the system. Assuming the sites on the chain are separated by a distance a we write the Fourier transform of $\hat{c}_n^\dagger$ and $\hat{c}_n$ as

$$\hat{c}_k = \frac{\sqrt{a}}{\sqrt{2\pi}} \sum_{n\in\mathbb{Z}} \hat{c}_n e^{-ikna} \tag{120}$$

$$\hat{c}_k^\dagger = \frac{\sqrt{a}}{\sqrt{2\pi}} \sum_{n\in\mathbb{Z}} \hat{c}_n^\dagger e^{ikna}. \tag{121}$$

The inverse Fourier transformation can be calculated accordingly.

$$\hat{c}_n = \frac{\sqrt{a}}{\sqrt{2\pi}} \int_{-\pi/a}^{\pi/a} \mathrm{d}k \hat{c}_k e^{ikna} \tag{122}$$

$$\hat{c}_n^\dagger = \frac{\sqrt{a}}{\sqrt{2\pi}} \int_{-\pi/a}^{\pi/a} \mathrm{d}k \hat{c}_k^\dagger e^{-ikna} \tag{123}$$

It should be noted that the we assume the chain to be infinitely long leading to continuous values for k in momentum space whereas in position space the values for n are discrete. This explains why we have a sum in one case and an integral over the Brillouin zone in the other. The on site energy in (119) is represent by the first term which gives a constant contribution which we will disregard. Now with the help of (120) and (123) we get

$$\hat{H} = -J \sum_{n\in\mathbb{Z}} \left(\hat{c}_n^\dagger \hat{c}_{n+1} + \hat{c}_{n+1}^\dagger \hat{c}_n\right) \tag{124}$$

$$= -J \sum_{n\in\mathbb{Z}} \frac{\sqrt{a}}{\sqrt{2\pi}} \left(\int_{-\pi/a}^{\pi/a} \mathrm{d}k \hat{c}_k^\dagger e^{-ikna} \hat{c}_{n+1} + \int_{-\pi/a}^{\pi/a} \mathrm{d}k \hat{c}_k^\dagger e^{-ik(n+1)a} \hat{c}_{n+1}\right) \tag{125}$$

$$= -J \int_{-\pi/a}^{\pi/a} \mathrm{d}k (\underbrace{e^{ika} + e^{-ika}}_{2\cos(ka)}) \hat{c}_k^\dagger \hat{c}_k \tag{126}$$

Now in order to generalize this result to two dimensions we have to introduce new operators $\hat{c}_{n,m}$ and $\hat{c}_{n,m}^\dagger$ due to fact that we now consider a square lattice with lattice sites located at (na,ma). The Hamiltonian can be split in terms representing tunneling in $x-$

and or y-direction.

$$\hat{H} = -J \sum_{n\in\mathbb{Z}} \sum_{m\in\mathbb{Z}} \left(\hat{c}^\dagger_{n,m+1}\hat{c}_{n,m} + \hat{c}^\dagger_{n,m}\hat{c}_{n,m+1} + \hat{c}^\dagger_{n+1,m}\hat{c}_{n,m} + \hat{c}^\dagger_{n,m}\hat{c}_{n+1,m} \right) \tag{127}$$

$$= -J \sum_{n\in\mathbb{Z}} \sum_{m\in\mathbb{Z}} \left(\hat{c}^\dagger_{n,m+1}\hat{c}_{n,m} + \hat{c}^\dagger_{n,m}\hat{c}_{n,m+1} \right) - J \sum_{m\in\mathbb{Z}} \sum_{n\in\mathbb{Z}} \left(+\hat{c}^\dagger_{n+1,m}\hat{c}_{n,m} + \hat{c}^\dagger_{n,m}\hat{c}_{n+1,m} \right) \tag{128}$$

The Fourier transformation can be performed similarly to the 1D case but two momenta k_x and k_y are required and the Fourier transform only acts on of the two coordinates. With (126) this leads to

$$\hat{H} = \sum_{n\in\mathbb{Z}} \int_{-\pi/a}^{\pi/a} \mathrm{d}k_y \left(-2J\cos k_y a\right) \hat{c}^\dagger_{n,k_y}\hat{c}_{n,k_y} + \sum_{m\in\mathbb{Z}} \int_{-\pi/a}^{\pi/a} \mathrm{d}k_x \left(-2J\cos k_x a\right) \hat{c}^\dagger_{k_x,m}\hat{c}_{k_x,m} \tag{129}$$

$$= \int_{-\pi/a}^{\pi/a} \mathrm{d}k_x \int_{-\pi/a}^{\pi/a} \mathrm{d}k_y \left(-2J(\cos k_x a + \cos k_y a)\right) \hat{c}^\dagger_{k_x,k_y}\hat{c}_{k_x,k_y} \tag{130}$$

Now we will introduce an additional magnetic phase ϕm to the terms related to tunneling in x-direction. The Hamiltonian from (127) can be modified to reflect those phases.

$$\hat{H} = -J \sum_{n\in\mathbb{Z}} \sum_{m\in\mathbb{Z}} \left(\hat{c}^\dagger_{n,m+1}\hat{c}_{n,m} + \hat{c}^\dagger_{n,m}\hat{c}_{n,m+1} + e^{-i\phi m}\hat{c}^\dagger_{n+1,m}\hat{c}_{n,m} + e^{i\phi m}\hat{c}^\dagger_{n,m}\hat{c}_{n+1,m} \right) \tag{131}$$

$$= \int_{-\pi/a}^{\pi/a} \mathrm{d}k_x \int_{-\pi/a}^{\pi/a} \mathrm{d}k_y \left(-2J + \cos\left(k_y a\right)\right) \hat{c}^\dagger_{k_x,k_y}\hat{c}_{k_x,k_y} + \sum_{m\in\mathbb{Z}} \int_{-\pi/a}^{\pi/a} \mathrm{d}k_x \left(-2J\cos\left(k_x a + \phi m\right)\right) \int_{-\pi/a}^{\pi/a} \frac{\mathrm{d}k_y a}{2\pi} \int_{-\pi/a}^{\pi/a} \mathrm{d}k'_y e^{-i(k_y - k'_y)ma} \hat{c}^\dagger_{k_x,k_y}\hat{c}_{k_x,k'_y} \tag{132}$$

The term $\cos\left(k_x a + \phi m\right)$ is of special interest to us. Suppose $\phi/(2\pi) = p/q$ is a rational number and p and q are coprime then $\cos\left(k_x a + \phi m\right)$ can only take q different values. This shows similarities with the Energy spectrum. In the Hofstadter butterfly we have q different bands for $\Phi/2\pi = p/q$. The calculations for the 2D square lattice can be easily extended to a rectangular one by introducing a_x and a_y as two lattice constants. The case for $a_x = a_y$ $\phi = p/q$ has similarities to the case $a_x = q a_y$ with $\phi = 0$. This is due to fact that in the first case a particle traveling along the sides around of the unit cell of the second case picks up a phase of $p \cdot 2\pi$.

Since we were able to diagonalize the Hamiltonian for the $\phi = 0$ case we can now use this result to calculate the time evolution of a particle on the lattice. Again we start by looking at the one dimensional case. Suppose we start at $t = 0$ with the state localized around the site m_0

$$|\Psi(0)\rangle = |n_0\rangle = \hat{c}_{n_0}|vac\rangle \tag{133}$$

The state at a later time t can be calculated as

$$\Psi(t) = U(t)\,|n_0\rangle \tag{134}$$

$$= e^{-i\hat{H}t/\hbar}\,|n_0\rangle \tag{135}$$

By changing into Fourier space with states $|k\rangle$ we can make use of the fact that from (126) follows $\hat{H}\,|k\rangle = 2J\cos(ka)\,|k\rangle$. This leads to

$$\Psi(t) = \frac{\sqrt{a}}{\sqrt{2\pi}} \int_{-\pi/a}^{\pi/a} \mathrm{d}k e^{ikn_0a} e^{-it\hat{H}/\hbar}\,|k\rangle \tag{136}$$

$$= \frac{\sqrt{a}}{\sqrt{2\pi}} \int_{-\pi/a}^{\pi/a} \mathrm{d}k e^{ikn_0a} e^{i2Jt\cos ka/\hbar}\,|k\rangle\,. \tag{137}$$

Here we can make use of the Jacobi-Anger expansion it relates $\cos(z)$ with the n-th Bessel functions of the first kind.

$$e^{iz\cos\alpha} = \sum_{n\in F} i^n J_n(z) e^{in\alpha} \tag{138}$$

Plugging (138) into (137) yields

$$\Psi(t) = \frac{\sqrt{a}}{\sqrt{2\pi}} \int_{-\pi/a}^{\pi/a} \mathrm{d}k \left(\sum_{m\in\mathbb{Z}} i^m J_m(2Jt/\hbar) e^{ikam} \right) e^{ikn_0a}\,|k\rangle \tag{139}$$

$$= \sum_{m\in\mathbb{Z}} i^m J_m(2Jt/\hbar)\,|m+n_0\rangle \tag{140}$$

$$= \sum_{n\in\mathbb{Z}} i^{n-n0} J_{n-n0}(2Jt/\hbar)\,|n\rangle \tag{141}$$

This result can be easily extended to the two dimensional case. Since the Hamiltonian from (129) can be written as $\hat{H} = \hat{H}_x + \hat{H}_y$ where each part only acts on its subspace. Multiplying the prefactors from each subspace the two dimensonal version of (141) reads

$$\Psi(t) = \sum_{n\in\mathbb{Z}} \sum_{m\in\mathbb{Z}} i^{n+m-n_0-m_0} J_{n-n0}(2Jt/\hbar) J_{m-m0}(2Jt/\hbar)\,|n,m\rangle \tag{142}$$

This enables us to calculate the mean distance from the starting point as a function of t.

$$x_{mean}(t) = \sum_{n\in\mathbb{Z}} \sum_{m\in\mathbb{Z}} \left(J_{n-n_0}(2Jt/\hbar) J_{m-m_0}(2Jt/\hbar)\right)^2 \sqrt{(n-n_0)^2 + (m-m_0)^2} \tag{143}$$

Now we are going to consider the case where no lattice is present. Consider a Gaussian wave packet located around the origin at (t=0)

$$\Psi(x,y,0) = \frac{1}{\sqrt{\pi a}} e^{-\frac{x^2+y^2}{2a}}. \tag{144}$$

The particle is free not restricted onto a lattice. Nonetheless we can proceed by Fourier transforming (144).

$$\Psi(k_x,k_y,0) = \sqrt{\frac{a}{\pi}} e^{-a\frac{k_x^2+k_y^2}{2}}. \tag{145}$$

Each k state evolves with $\exp(-itE_k/\hbar)$ with $E_k = \hbar^2(k_x^2+k_y^2)/(2m)$. By inverse Fourier

transform this yields the time evolved wave packet as

$$\Psi(x,y,t) = \sqrt{\frac{a}{\pi}} \int_{-\infty}^{\infty} \frac{\mathrm{d}k_x}{\sqrt{2\pi}} \int_{-\infty}^{\infty} \frac{\mathrm{d}k_y}{\sqrt{2\pi}} e^{(-it(\hbar(k_x^2+k_y^2)/(2m))} e^{-a\frac{k_x^2+k_y^2}{2}} e^{ik_x x} e^{ik_y y} \tag{146}$$

$$= \frac{1}{\sqrt{a\pi}} \frac{1}{1+\frac{it\hbar}{2m}} e^{-\frac{x^2+y^2}{2a(1+\frac{it\hbar}{2m})}} \tag{147}$$

from this we can calculated the mean distance from the origin as

$$x_{mean} = \sqrt{\langle x^2 \rangle} = \sqrt{\frac{a}{2}\left(1+\left(\frac{\hbar t}{ma}\right)^2\right)} \tag{148}$$

For large t (148) grows linearly in time as $\frac{\hbar t}{m\sqrt{a}}$. The factor $\frac{1}{\sqrt{a}}$ implies that the stronger the wave packet is localized for $t = 0$ the faster it spreads. This can be explained by the fact that a small spatial uncertainty is linked with a large uncertainty in momentum.
In classical systems spreading is usually sub-linear. A suitable example for this would be the random walk of a particle on a two dimensional square lattice. Suppose the particle jumps with equal probability in each direction, then the question of interest is how far on average is it separated from its origin after N jumps? This can be done by summing taking the average over all distances to the origin for the paths of length N. This leads to the asymptotic behaviour $x_{mean}(N) \propto \sqrt{N}$.
This indicates that classical random walks are not a suitable tool to describe the spreading of quantum systems. Fortunately we can resort to the quantum equivalent the quantum random walk.

5.2. Numerical Approach Using Continuous Quantum Random Walks

In this section we will only give a very brief introduction into the theory of quantum random walks. A detailed introduction into this topic is given in [12]. There are two types of quantum random walks the discrete and the continuous quantum random walk.

In the discrete quantum random walk one can define a step operator $\hat{S}$ and coin operator $\hat{C}$. The evolution of the wave function with respect to the amount of jumps N can be calculated as

$$|\Psi(N)\rangle = (\hat{S} \cdot \hat{C})^N |\Psi(0)\rangle . \tag{149}$$

A standard example for the discrete quantum walk would be the Hadamard coin in one dimension. However the version we are going to use is the continuous quantum random walk. First consider a finite undirected graph and a constant tunnel rate J. We start off by labeling all vertices with numbers 0 to n this allows to calculate the adjacency matrix of the graph.

$$A_{ij} = \begin{cases} 1 & i,j \text{ are connected} \\ 0 & \text{else} \end{cases} \tag{150}$$

In our case we take a finite section of a square lattice as a graph by only connecting those vertices which correspond to neighboring lattice sites we restrict ourselves to nearest

neighbor tunneling. The degree matrix is defined by

$$D_{ij} = \begin{cases} deg(i) & i = j \\ 0 & \text{else} \end{cases} . \tag{151}$$

The degree of $\deg(i)$ of a vertex represents the number of vertices connected to it. The Lagrangian matrix is defined as $L = A - D$. The adjacency matrix represent tunneling whereas the degree matrix represents the on site energy. In the continuous time quantum random walk we replace the Hamiltonian in the time evolution operator with $\hat{H} = -JL$. The time evolution then becomes

$$|\Psi(t)\rangle = e^{iJtL/\hbar} |\Psi(0)\rangle \tag{152}$$

In [11] the continuous quantum random walk is explained in more detail and applied to different types of lattices. Our main interest will lay in the regime for large t. For simplicity's sake we will from here on out express t in units of $\hbar$ as $T = t/\hbar$ and investigate the time evolution as a function of JT.

The finite size of the graph should be chosen in such a way that finite size effects are minimized, while keeping the computation times reasonably low. It is sensible to chose the initial state as the vertex in the center of the chosen graph to further reduce finite size effects. The case where no magnetic phases are present serves as good consistency check since we know the analytical result from (142). The results for a 61×61 grid are depicted in figure 6.

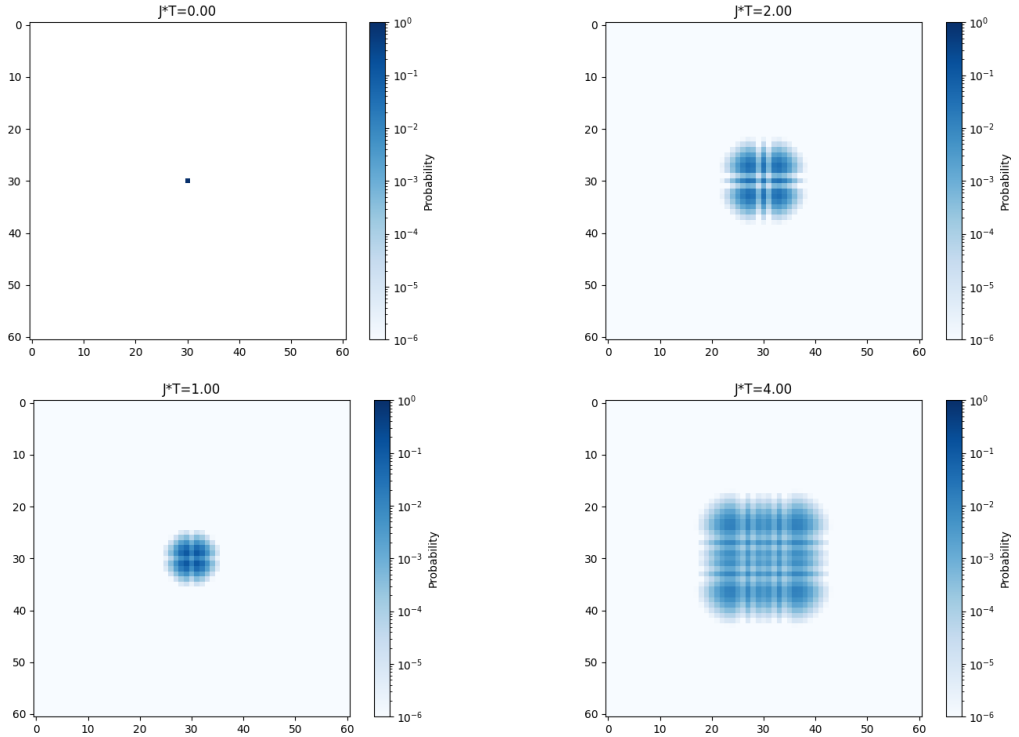

Figure 6: Shown is the probability distribution of a particle on a square lattice for $Jt =$ 0,1,2 and 4. The scale is logarithmic as the probabilities in span across multiple orders of magnitude

Looking at figure 6 one can easily check the consistency with equation (142) by comparing the zeroes of the Bessel functions with the stripes of low probability present in the pictures. $J_0(2JT)$ has its first positive zero for $JT \approx 1{,}20$ explaining the stripes of low probability which go through the origin ((30,30) in figure6) as seen in the picture for $JT = 1$. The first positive zero of $J_1(2JT)$ and $J_{-1}(2JT)$ are at $JT \approx 1{,}91$. Looking at the probability distribution for $JT = 2$ there are two horizontal and vertical stripes visible passing exactly next to the origin. This Process can repeated for other zeroes of the Bessel functions and confirming that the zeroes from the analytical calculations do in fact coincide with the stripes of low probability in the numerical results.

As a next step we can check whether x_{mean} does in fact grow linear in JT. The function $x_{mean}(JT)$ is plotted in figure 7.

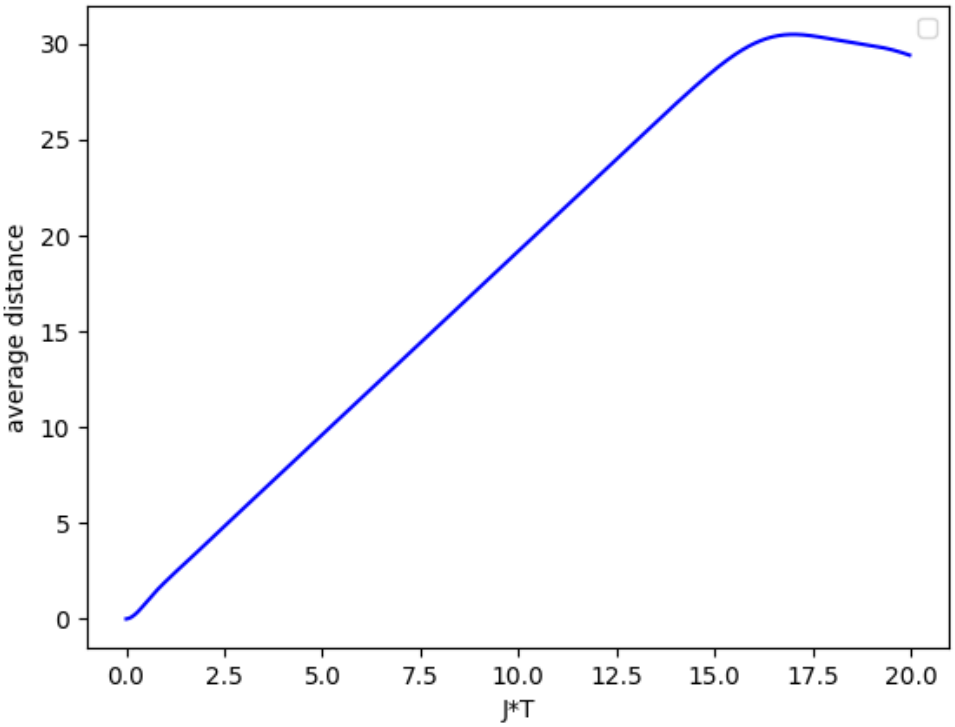

Figure 7: Shown is the average distance x_{mean} as function of JT for $N = 61$.

Figure 7 shows the linear growth of x_{mean} quadratically faster compared to a particle performing a classical random walk. The reason x_{mean} stops growing at some point as seen in figure 7 is that the at some point a significant part of the wave function reaches the border of our finitely sized grid. In order to gauge the effect of finite size effects we can produce the same graph but for different grid sizes of $N \times N$. The result can be seen in figure 8.

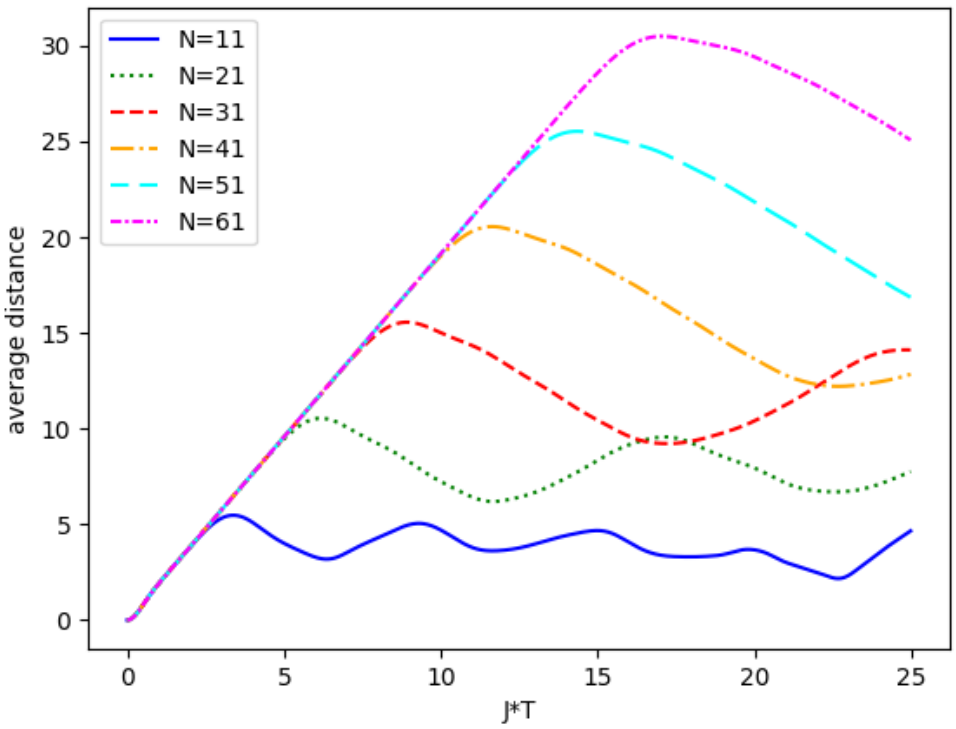

Figure 8: Shown is the average distance x_{mean} as function of JT for different values of N.

It is clear from figure 8 that the finite size effects x_{mean} when x_{mean} is getting close to $\frac{N}{2}$. Now we will return to the case where magnetic phases are present. The magnetic phases are multiplied to the corresponding terms in the adjacency matrix as a factor $e^{i\phi m}$. For the phase $\phi = \pi$ a lot of paths are destructively interfering with each other and canceling each other out completely. In 9 it can be seen that for all lattice sites where both coordinates are odd numbers the probability is zero for all JT. This can be explained by looking at all paths of given length connecting the starting point to the specific lattice site. For example there are two paths of length two connecting the starting point with a lattice site diagonally from it. Their contributions cancel each other since the phase difference leads to a factor $e^{-i\pi} = -1$ in front of one compared to the other. In the cases where more paths of higher length are possible we can group them into pairs canceling each other out. Note that this does only work if the paths are traveling an odd number of steps in both coordinates.

This effect can be observed for a more general array of phases. For magnetic phases $\phi = \pi/q$ where $q \in \mathbb{N}$ the same spots of with zero probability can be observed but spaced further apart. For the $\phi = \pi$ those spots are spaced two apart, for $\phi = \pi/q$ they are now spaced $2q$ apart. This effect does not generalize to all phases of the form $\phi = \pi \cdot (p/q)$. This can be seen in appendix C .

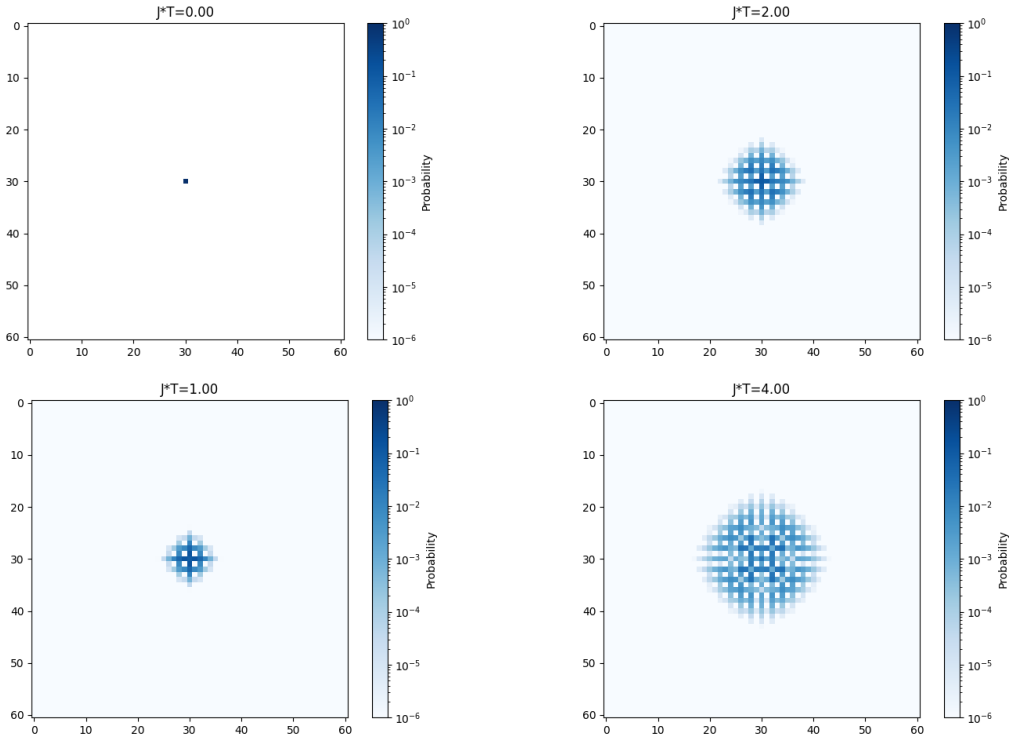

Figure 9: Shown is the probability distribution of a particle on a square lattice for $JT =$ 0,1,2 and 4. The magnetic phase per lattice cell is $\phi = \pi$

The next question is how does the magnetic phase influence x_{mean}. In figure 11 x_{mean} is plotted against JT for different values of ϕ. For large JT x_{mean} grows linear but the steepness of the graphs is heavily depended on ϕ. Finite size effects do again play a role here if JT grows large. When looking at the graphs in 10 it is visible that finite size effects can occur as early as in the $\phi = 0$ case even tough x_{mean} is considerably smaller than $N/2$. Another effect which can be seen in figure 11 is that the closer ϕ is getting to π the stronger x_{mean} is decreased in the beginning. For larger JT this trend disappears and a more complicated situation arises. In order to visualize the dependence on ϕ we can fix JT at different values and plot x_{mean} as a function of ϕ over the interval [0,2π]. The resulting graphs are pictured in figure 12

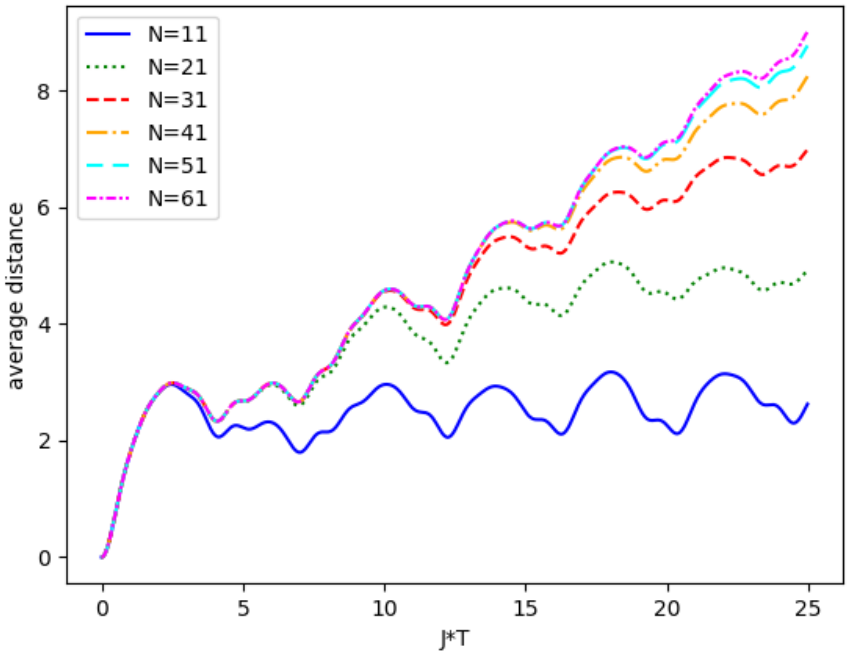

Figure 10: Shown is the average distance x_{mean} as function of JT for different values of N with $\phi = \pi/3$.

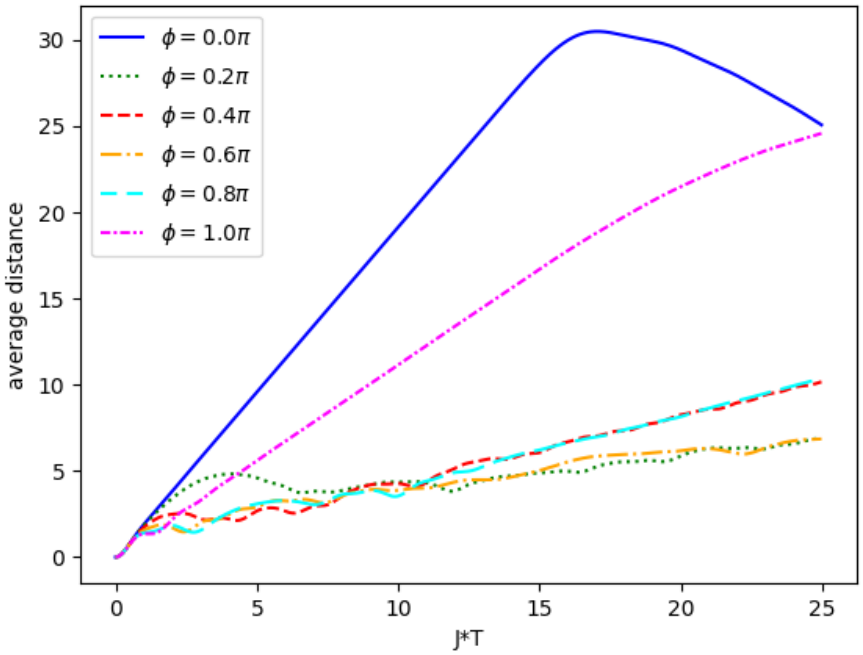

Figure 11: Shown is the average distance x_{mean} as function of JT for different values of ϕ for $N = 61$.

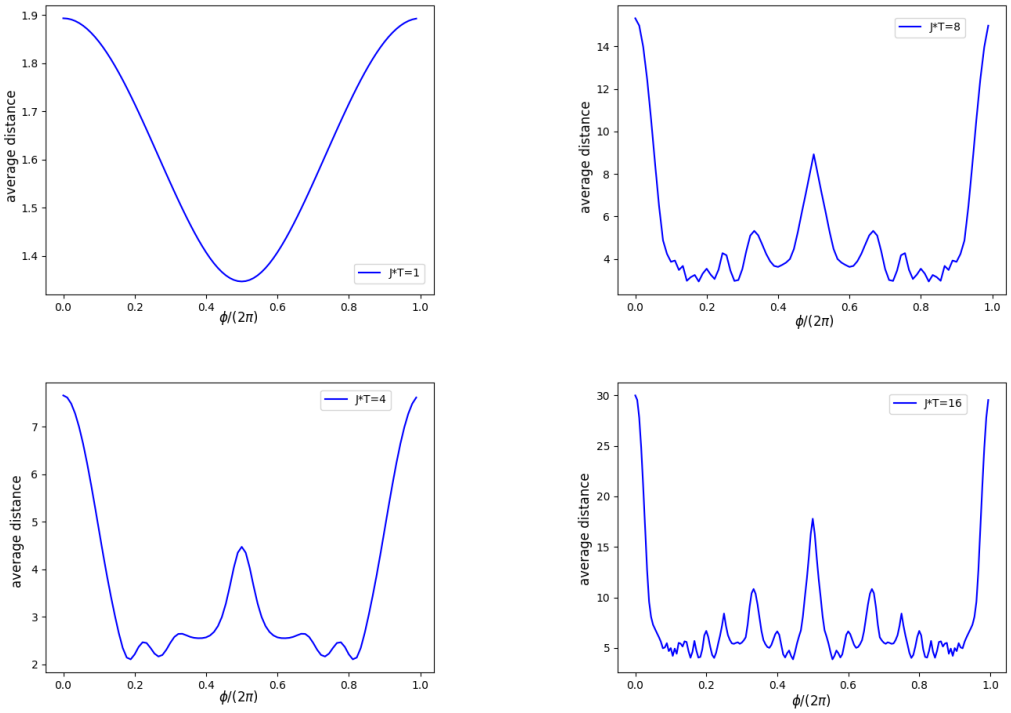

Figure 12: Shown is the average distance x_{mean} as function of ϕ for different values of JT.

Figure 12 shows that $x_{mean}(\phi)$=$x_{mean}(2\pi-\phi)$. For small JT $x_{mean}(\phi)$ is lower the closer it ϕ is to π confirming the trend seen already in figure 11. For large JT a different more complex picture starts to arise. $x_{mean}(\phi)$ is now dependent on the rationality of $\phi/2\pi$. More precisely the closer $\phi/2\pi$ is to a rational number p/q with low q the higher is x_{mean}.p however has no significant impact in this regime as $x_{mean}(2\pi(p/q)) \approx x_{mean}(2\pi)/q$. The numerical results suggest that for $\phi = 2\pi$ $x_{mean}(JT) \approx 2JT$ .Here we can remind ourselves that for such magnetic phases we can define a larger unit cell by putting q unit cells next to each other. A path around this new unit cell now picks up a phase of $2\pi p$. This peculiar dependency on the rationality of physical quantity is owed to the specific underlying system. We see a similar effect in the energy spectrum of the Hofstadter butterfly as pointed out [9]. Every irrational number can be arbitrarily close approximated using rational numbers. Together with the fact that a physical quantity like ϕ is subject to uncertainty we can deduct that for finite JT the behaviour even for irrational $\phi/2\pi$ is governed by the rational numbers in close proximity. A similar for $JT = 25$ is shown in appendix C

It is clear that the dependence on ϕ relies on the presence of a lattice, when comparing with the results for the free particle we see that this behaviour can not be present in the limit $V_0 \to 0$ even though J does not depend on V_0 in the instanton approximation.

6. Conclusion

We start this chapter by giving short summary highlighting how the calculations from the different chapters are connected. In chapter 2 we found that a electron moving through a magnetic field is equivalent to a neutral particle in a rotating trap. The correspondence in this case is $2m\omega \leftrightarrow eB$. After introducing cyclotron and guiding center coordinates we restrict the particle into the lowest Landau level connected to cyclotron coordinates. This allows us to project the added potential in such a way that is now only a function of guiding center coordinates namely $V_0(2 - \cos(x/a) - \cos(x/a))$. The instanton found suggest that the tunnel rate between the different minima does not depend on V_0. What we are left with is a time evolution which is governed by the geometry of the lattice. A key role here plays the Aharanov-Bohm phase for a rotating trap we get a similar phase since the phase is caused by the non commutative nature of the coordinates which is present in both cases. The numerical analysis shows that the long term behaviour when it comes to spreading on the lattice depends on the rationality of $\phi/2\pi$. Now if we return back into the original coordinates we have $x = \xi + X$ and $y = \nu + Y$, the geometry of V and $\tilde{V}$ is the same. A tunneling event $X \to X + 2\pi a$ can written in the original coordinates as $x = \xi + X \to \xi + X + 2\pi a$. Tunneling in the guiding center coordinates can be viewed as changing from one Landau orbit into another orbit around a different center.

It would be interesting to see if it is possible to realize a system, in which our theoretical predictions concerning the spreading could be measured. Concretely by applying a suitable external periodic potential and checking whether there is a regime in which changing the amplitude of the potential does not affect the speed with which a localized state spreads. Additionally the influence of the spacing of the potential could be investigated. Measuring the effects of the phases connected to the magnetic field or rotation frequency on the time evolution is likely to be challenging.

References

[1] Richard J. Fletcher, Airlia Shaffer, Cedric C. Wilson et al. Geometric squeezing into the lowest Landau level, Science Vol 372, Issue 6548 pp. 1318-1322 July 1 2021.

[2] M. M. Mizrahi, The Weyl correspondence and path integrals , J. Math. Phys. 16, 2201, 1975. https://doi.org/10.1063/1.522468

[3] R. MacKenzie, Path Integral Methods and Applications, April 24 2000. https://doi.org/10.48550/arXiv.quant-ph/0004090

[4] D.Tong, The Quantum Hall Effect, September 20 2016. https://doi.org/10.48550/arXiv.1606.06687

[5] Duan, Z., Gu, J., Hatsuda, Y. et al. Instantons in the Hofstadter butterfly: difference equation, resurgence and quantum mirror curves. J. High Energ. Phys. 2019, 79, January 9 2019. https://doi.org/10.1007/JHEP01(2019)079

[6] D. Freed, J. A. Harvey, Instantons and the spectrum of Bloch electrons in a magnetic field Phys. Rev. B 41, 11328, June 1 1990.

[7] J. K. Jain, S. Kivelson, Model tunneling problems in a high magnetic field, Phys. Rev. B 37, 4111, March 15 1988.

[8] S. Coleman, The Uses of Instantons, Subnucl.Ser. 15 (1979) 805, February 1978.

[9] D.R.Hofstadter, Energy levels and wave functions of Bloch electrons in rational and irrational magnetic fields, Physical Review B Vol 14, Number 6, September 15 1976.

[10] B.Sakita Quantum Theory of Many-variable Systems and Fields, World Scientific Lecture, Notes Vol.1, 1985.

[11] L. Razzoli, M. G. A. Paris, P. Bordone, Continuous-time quantum walks on planar lattices and the role of the magnetic field, Phys. Rev. A 101, 032336, March 23 2020.

[12] J. Kempe, Quantum random walks: An introductory overview, Contemporary Physics: Vol. 44, No. 4, pp. 307-327, August 2003.

A. Identity for Hermite Polynomials

Let us define $W[f(x)]$ as the transformation

$$\int_{-\infty}^{\infty} \frac{e^{-R^2}}{\sqrt{\pi}} f(x+R)\mathrm{d}R. \tag{153}$$

The identity we want to prove is the following

$$W\left[\frac{H_n(x)}{2^n}\right] = x^n \tag{154}$$

where $H_n(x)$ is the n-Hermite polynomial. This can be done via proof by induction. For $n = 0$ we have

$$W\left[\frac{H_0(x)}{2^0}\right] = \int_{-\infty}^{\infty} \frac{e^{-R^2}}{\sqrt{\pi}}\mathrm{d}R = 1 = x^0 \tag{155}$$

and for $n = 1$ we get

$$W\left[\frac{H_1(x)}{2}\right] = \int_{-\infty}^{\infty} \frac{e^{-R^2}}{\sqrt{\pi}}(x+R)\mathrm{d}R = x. \tag{156}$$

Now suppose equation (154) is true for n as well as $n-1$. Using the identities $H_{n+1} = 2xH_n(x) - 2nH_{n-1}(x)$ and $H_n'(x) = 2nH_{n-1}(x)$ we get

$$W\left[\frac{H_{n+1}(x)}{2^{n+1}}\right] = \frac{1}{2}\int_{-\infty}^{\infty} \frac{e^{-R^2}}{\sqrt{\pi}} \frac{H_{n+1}(x+R)}{2^n}\mathrm{d}R \tag{157}$$

$$= \frac{1}{2}\int_{-\infty}^{\infty} \frac{e^{-R^2}}{\sqrt{\pi}} \frac{2(x+R)H_n(x+R) - 2nH_{n-1}(x+R)}{2^n}\mathrm{d}R \tag{158}$$

$$= xW\left[\frac{H_n(x)}{2^n}\right] - \frac{n}{2}W\left[\frac{H_{n-1}(x)}{2^{n-1}}\right] + \int_{-\infty}^{\infty} \frac{e^{-R^2}}{\sqrt{\pi}} \frac{RH_n(x+R)}{2^n}\mathrm{d}R \tag{159}$$

$$= x^{n+1} - \frac{n}{2}x^{n-1} + \underbrace{\left[\frac{-H_n(x+R)e^{-R^2}}{2^{n+1}\sqrt{\pi}}\right]_{-\infty}^{\infty}}_{=0} - \underbrace{\int_{-\infty}^{\infty} \frac{2nH_{n-1}(x+R)}{2^n\sqrt{\pi}} \frac{-e^{-R^2}}{2}\mathrm{d}R}_{=-(n/2)x^{n-1}} \tag{160}$$

$$= x^{n+1}. \tag{161}$$

By Induction we have now proven (154) for all $n \in \mathbb{N}_0$.

B. Calculating Functional Determinants

When calculating the partition function in the instanton formalism we are often faced with quotients of functional determinants. In this section we explain how such terms can be evaluated without having to calculate the entire spectrum of the operators. This method is used in [5], [8] and [10].
Consider the quotient

$$\frac{\det(-\frac{\mathrm{d}}{dx^2}+V_1(x)-z)}{\det(-\frac{\mathrm{d}}{dx^2}+V_2(x)-z)} \tag{162}$$

where $z \in \mathbb{C}$. Now we try to find two meromorphic functions Ψ_1^z and Ψ_2^z which satisfy the following three conditions.

$$\left(-\frac{\mathrm{d}}{dx^2}+V_i(x)-z\right)\Psi_i^z(x) = 0 \tag{163}$$

$$\Psi_i^z(0) = 0 \tag{164}$$

$$\frac{\mathrm{d}\Psi_i^z}{dx}(0) = 1 \tag{165}$$

The quotient of those two function can be used do define a function on $\mathbb{C}$.

$$F(z) = \frac{\Psi_1^z(L)}{\Psi_2^z(L)} \tag{166}$$

Now we can compare the expressions in (162) and (166). We see that they have the same zeroes. If z is an eigenvalue of $-\frac{\mathrm{d}}{dx^2}+V_1(x)$ then $\Psi_1^z(x)$ is an eigenfunction of $-\frac{\mathrm{d}}{dx^2}+V_1(x)$ from which we can follow that $\Psi_1^z(L)=0$. The same argument can be repeated for the denominator which shows that they also have the same poles. Now we can apply Riemann's theorem on removable singularities. If we can show that the quotient of (162) and (166) is bounded then Liouville's theorem tells us that the quotient has to be constant. Therefore (162) and can only differ by a constant factor from (166). For appropriate conditions which we have chosen this factor is 1. Resulting in

$$F(z) = \frac{\Psi_1^z(L)}{\Psi_2^z(L)} = \frac{\det(-\frac{\mathrm{d}}{dx^2}+V_1(x)-z)}{\det(-\frac{\mathrm{d}}{dx^2}+V_2(x)-z)}. \tag{167}$$

This reduces the problem from having to calculate functional determinants to solving differential equations with appropriate boundary conditions. Note that if one operator has a zero mode, this zero mode has to be treated separately.

C. Additional Figures for Different Phases and Longer Times

In this section a few additional figures are presented. Figure 13 shows the probability distribution for $\phi = \pi/3$ at different times. On closer examination we can make out lattice sites of zero probability which stay the same for all JT and are spaced 6 sites apart from the next ones. As a comparison we can look at figure 14 where the corresponding pictures for $\phi = 2\pi/3$ are shown. In figure 14 are no lattice sites where the probability vanishes.

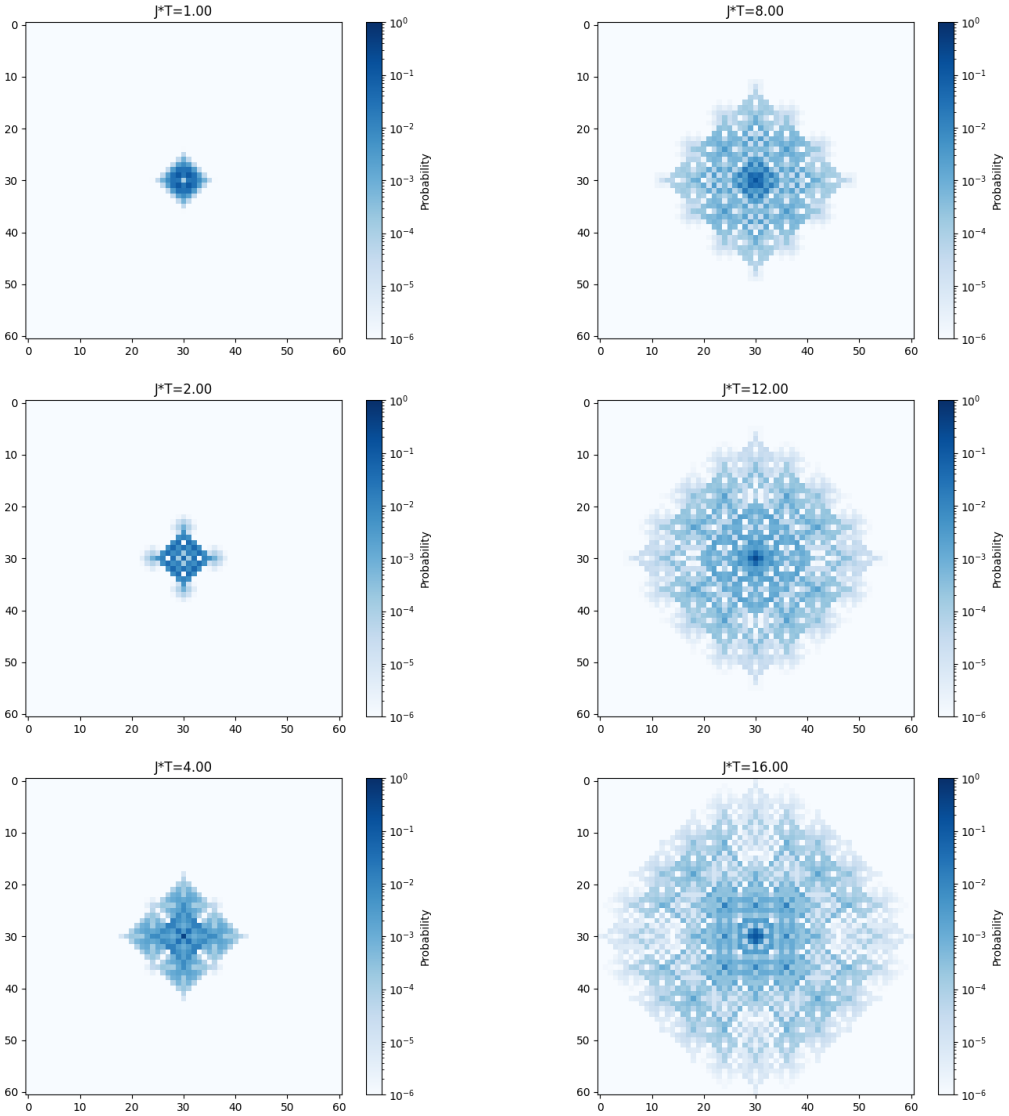

Figure 13: Shown is the probability distribution of a particle on a square lattice for $JT = 1,2,4$ and 8. The magnetic phase per lattice cell is $\phi = \pi/3$

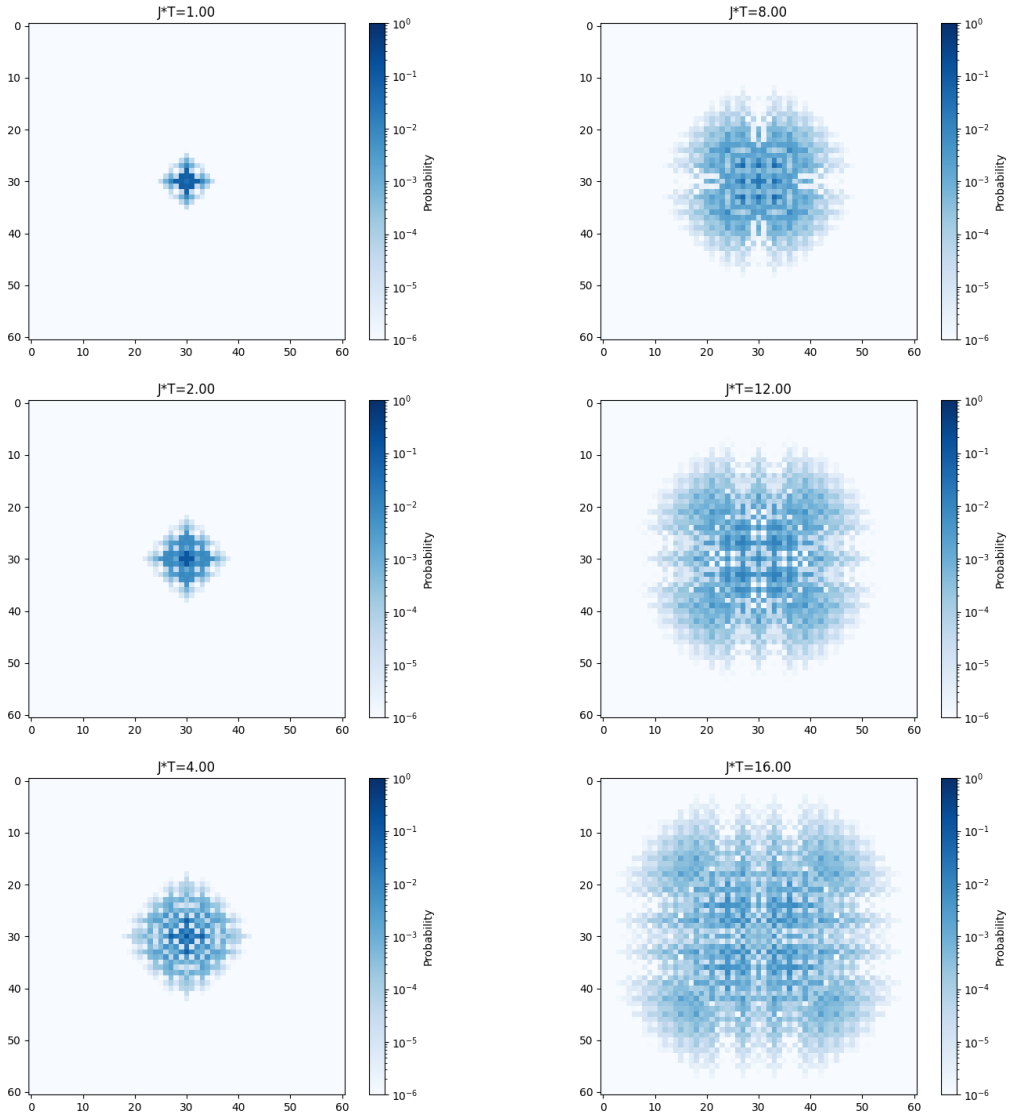

Figure 14: Shown is the probability distribution of a particle on a square lattice for $JT = 1,2,4$ and 8. The magnetic phase per lattice cell is $\phi = 2\pi/3$

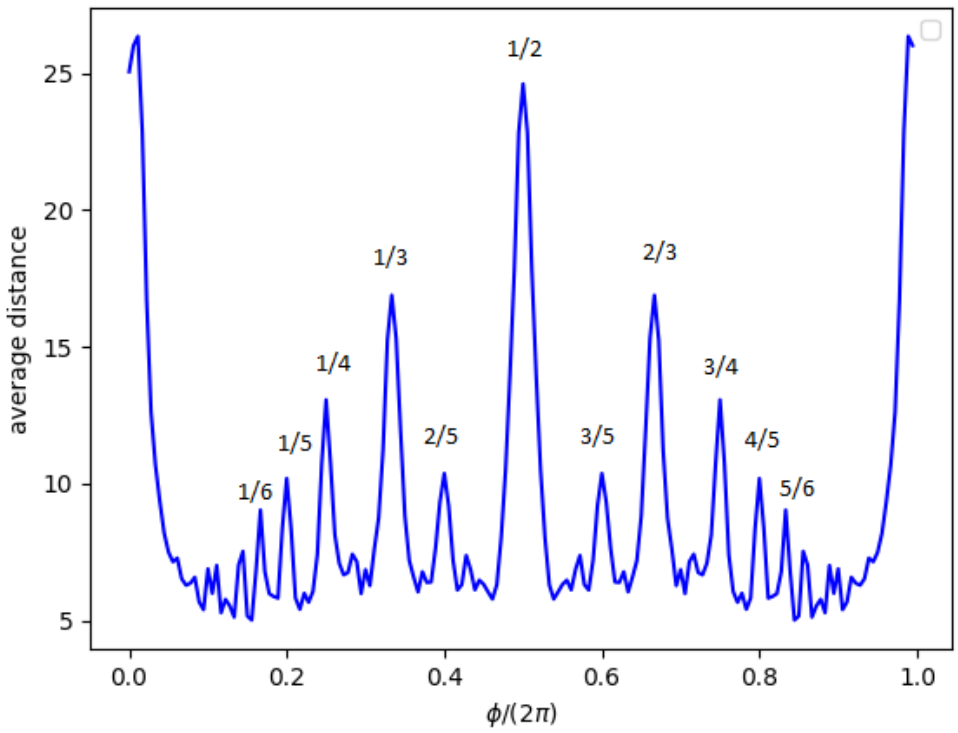

Figure 15: Shown is the average distance x_{mean} as function of $\phi/2\pi$ for $JT = 25$ and $N = 61$.

In figure 15 we have plotted x_{mean} against $\phi/2\pi$ for $JT = 25$. The peaks for $\phi/2\pi = p/q$ with small q are very pronounced and can be labeled accordingly. Here JT is so large that finite size effects play a role which can be seen for ϕ close to 0 and close to 2π.